Mechanistic Study of Pyrolysis of Small Boron Hydrides

by

Baili Sun

A thesis submitted to the Graduate Faculty of
Auburn University
in partial fulfillment of the
requirements for the Degree of
Master of Science

Auburn, Alabama
August 3, 2013

Keywords: Mechanism, Boron Hydrides, Kinetics

Approved by

Michael L. McKee, Chair, Professor, Department of Chemistry and Biochemistry
David M. Stanbury, Professor, Department of Chemistry and Biochemistry
German Mills, Associate Professor, Department of Chemistry and Biochemistry

Abstract

Theoretical background and computational methods are introduced in Chapter 1. In Chapter 2 the rate constant for the association of two boranes to form diborane is investigated using several methods. The most sophisticated method is variable reaction coordinate - variation transition state theory (VRC-VTST) which has been developed to handle reactions with no enthalpic barriers. The rate constant was computed using conventional VTST with the IRC from the G4 and W1DB methods. Two variations of the multi-step mechanisms for diborane pyrolysis are presented.

The initial steps in the B_4H_{10} pyrolysis mechanism have been elucidated in Chapter 3. The mechanism can be divided into three stages: initial formation of B_4H_8, production of volatile boranes with B_3H_7 acting as a catalyst, and formation of nonvolatile products. The first step is B_4H_{10} decomposition to either B_4H_8/H_2 or B_3H_7/BH_3 where the free energy barrier for the first pathway is 5.6 kcal/mol higher (G4, 333 K) than the second pathway when transition state theory (TST) is used. We suggest that the rate-determining step is $B_4H_{10} + B_3H_7 \rightarrow B_4H_8 + H_2 + B_3H_7$ where B_3H_7 acts as a catalyst. The role of reactive boron hydrides such as B_3H_7 and B_4H_8 as catalysts in the build-up of larger boron hydrides may be more common than that previously considered.

Acknowledgments

I would like to acknowledge Prof Michael L. McKee. This thesis would not have been possible without his support and guidance. He continually conveyed a spirit of excellence to me in regard to research and study. I am also very grateful to Dr. Nida McKee for her help in my graduate life in Auburn.

I also thank my committee members, Prof. David M. Stanbury and Prof. German Mills for their persistent help towards my thesis.

Finally, I would like to thank my father Chuanlin Sun and my mother Shuhua Yang for their endless love and full support.

Table of Contents

List of Figures

List of Abbreviations

List of Tables

HF	Hartree-Fock
STO	Slater-type Orbital
GTO	Gaussian-type Orbital
CBS	Complete Basis Set
TST	Transition State Theory
VTST	Variational Transition State Theory
GTST	Generalized Transition State Theory
IRC	Intrinsic Reaction Coordinate
MEP	Minimum-energy Path
VRC	Variable Reaction Coordinate

Chapter 1

General Introduction

Computational chemistry has developed into a standard tool to understand chemical phenomena at the electronic and molecular levels. Its application has spread to almost all areas of science and engineering such as quantum chemistry, molecular modeling, drug delivery, and hydrogen storage. Through investigating the structures and properties of intermediates and transition structures, reaction mechanisms can be elucidated.

1.1 Schrödinger equation

The Schrödinger equation is the essential equation of quantum mechanics.[1,2] This second order partial differential equation determines how a physical system evolves in time. The Schrödinger equation in quantum mechanics is an analogy of Newton's law in classical mechanics.

The Schrödinger equation can be divided into two general subcategories: time-dependent and time-independent.

Time-dependent Schrödinger equation:

$$i\hbar\frac{\partial}{\partial t}\psi = \hat{H}\psi \qquad (1)$$

Time-independent Schrödinger equation:

$$E\psi = \hat{H}\psi \qquad (2)$$

1.2 The Born-Oppenheimer Approximation

The Born-Oppenheimer (BO) Approximation is indispensable in quantum chemistry.[3] It originates from the significant mass difference between nuclei and electrons. Since the nuclei are much heavier, their velocities are much smaller. Therefore, intuitively, the motion of electrons can be considered as circling mass points around the fixed nuclei. The Schrödinger equation is composed of two components. The electronic part describes the electronic wave function ($\psi_{\text{electronic}}$) depending only on electrons with fixed nuclei configuration. The nuclear part (vibrational, rotational) describes the nuclear wave function. For the general molecular system, the Schrödinger equation without electron effects can be drawn:

$$(T^{elec} + T^{nucl} + V^{nucl-elec} + V^{elec} + V^{nucl})\,\psi = E\psi \qquad (3)$$

T and V terms present kinetic and potential energies terms, respectively. The key point of the Born-Oppenheimer (BO) approximation is that it treats the two parts of the problem separately. Therefore, an electronic Schrödinger equation can be constructed:

$$\hat{H}^{elec}\psi^{elec} = E^{elec}\psi^{elec} \qquad (4)$$

$$\hat{H}^{elec} = T^{elec} + V^{nucl-elec} + V^{elec} + V^{nucl} \qquad (5)$$

E^{elec} represents the potential energy surface which depends on the nuclear configuration. The Born-Oppenheimer approximation is ubiquitous. Only the eigenfunctions of H_2 can

be solved accurately without it. One limitation of Born-Oppenheimer approximation is that relativistic effects are ignored which is important for heavy atoms.

1.3 Hartree-Fock Theory (HF theory)

As one of the basic fundamental theories of quantum chemistry, the solution of the Hartree-Fock equation is the root for most advanced *ab-initio* methods which provide more accurate description for many electrons system.[1,4] One problem with HF theory is that electron correlation is ignored in multi-electron systems. Electron correlation is treated in an average way, in other words, each electron only interacts with a static electron cloud of all the other electrons. Therefore, the lowest energy from HF theory will be always greater than the true energy of the system on the basis of the variational principle.

The self-consistent field method is proposed to solve HF theory. The key idea is as follows: first, an initial electronic configuration of the wavefunction (typically the ground state) will be guessed, which is a product of single electron-electron wave function. Second, the effect of all the other electrons have been included in the effective potential which will be solved for a new one-electron wavefunction for atom i. The same procedure will be applied for the next electron. After all the electrons have been scanned, the above procedure is iterated until the one-electron wavefunctions reach convergence.

1.4 Basis set

Mathematically, any set of functions can be used as a basis set.[1-3,5] The definition of basis set in theoretical and computational chemistry is as follows: a basis set is a set of

functions (called basis functions) which are linear combinations used to create molecular orbitals (ψ_j),

$$\psi_j = \sum_{i=1}^{n} c_{ij}\, \chi_i \qquad (6)$$

where the coefficients c_{ij} are also called the molecular orbital expansion coefficients, which can be determined numerically using the variational principle. χ_i refers to an arbitrary function. Larger basis sets more accurately approximate the orbitals by imposing fewer restrictions on the locations of the electrons in space. Meanwhile, the energy converges towards the HF limit of the method more closely.

Slater-type orbitals (STOs)[6] and Gaussian-type orbitals (GTOs)[4] are the two types of orbitals in quantum chemistry. Historically, STOs are important. Their application is now limited since integrals of STOs are difficult to evaluate. GTOs are dominant orbitals in modern chemistry calculations. GTOs are based on STOs but have a radial term following the function e^{-r^2}, thus they are more efficient for computation than STOs. However, GTOs also exhibit a deficiency which can be summarized as: "No cusp at nucleus". The solution to this deficiency is to typically replace each STO with 3 or 6 GTOs.

There are several terms used to describe basis sets. The definition of minimal basis set is that one basis function is employed per atomic orbital. For example, for CH_4, a 1s orbital is used for each H while 1s, 2s, 2px, 2py and 2pz orbital are employed for the atom C. Minimal basis sets can not describe the wavefunction sufficiently since the number and size of the orbitals are fixed for all systems. To improve the performance of

the minimal basis set, the number of basis functions for each orbital with different orbital exponents has been doubled and tripled, called Double-Zeta and Triple-Zeta, respectively. Usually, it is time-consuming to calculate a double-zeta basis set for every orbital. In chemical bonding, the core orbitals only weakly affect bonding properties while valence orbitals are very important. Split valence basis add additional flexibility for describing valence orbitals. Diffuse basis sets are applied to deal with systems that allow electrons to flow away from the nucleus, for instance, excited states and anions. Another modification of basis sets is to make the atomic orbitals polarized by the influence of their surroundings. Polarization basis set are usually presented as * or (d), for example, 6-31G(d) which is important for heavy atoms.

1.5 Composite method

The goal of the composite method is to model the thermochemical quantities accurately. Through combination of a series of different calculations an approximation to a higher level computation is made that would be very expensive in actual calculation, and high accuracy can be obtained. There are several families of the method: the Gaussian-n methods,[7-9] the Complete Basis Set (CBS) methods[10] and the W1 method.[11]

1.6 Fundamentals of kinetics

1.6.A Reaction Rates

For a general chemical reaction,

$$aA + bB \rightarrow pP + qQ \qquad (8)$$

the change of the reaction mixture with time is the reaction rate which is defined as:[12,13]

$$r = -\frac{1}{a}\frac{dA}{dt} = -\frac{1}{b}\frac{dB}{dt} = -\frac{1}{p}\frac{dQ}{dt} = -\frac{1}{q}\frac{dP}{dt} \quad (9)$$

The negative sign means the reactants are consumed; conversely, a positive sign indicates the concentrations of products are increasing.

1.6.B Reaction Laws and Reaction Order

For most reactions, the rates depend on the concentrations of one or more reactants or products. The exponents a, b, p and q may be integer, fractional, or negative while k is the rate constant. The equation is the rate equation or rate expression. The overall order of the reaction is simply the sum of exponents (a+b+p+q).

$$rate = k[A]^a[B]^b[P]^p[Q]^q \quad (10)$$

1.6.C Unimolecular Reactions

The elementary reaction step,

$$A \xrightarrow{k_1} B \quad (11)$$

is unimolecular since there is only one reactant while the rate law is

$$\frac{dB}{dt} = k_1[A] \tag{12}$$

Another simple unimolecular reaction may be described in fast equilibrium:

$$A \underset{k_2}{\overset{k_1}{\rightleftharpoons}} B \tag{13}$$

where A and B are isomers, for example, conformational or constitutional isomer. This reversible unimolecular step implies the following rate law,

$$\frac{dB}{dt} = k_1[A] - k_{-1}[B] \tag{14}$$

The system is in equilibrium, in other words, the reactant concentration is stationary, thus

$$\frac{k_1}{k_{-1}} = \frac{[B]_{eq}}{[A]_{eq}} = K_{eq} \tag{15}$$

A unimolecular reaction step can have more than one product such as in fragmentation.

$$A \overset{k_1}{\rightarrow} B + C \tag{16}$$

1.6.C Bimolecular Reactions

The bimolecular reaction

$$A + B \underset{k_{-2}}{\overset{k_2}{\rightleftarrows}} C \tag{17}$$

implies the rate law

$$\frac{dC}{dt} = k_2[A][B] - k_{-2}[C] \tag{18}$$

or it could be written as a rate of loss of A or B as we have seen above. The reversible bimolecular reaction,

$$A + B \underset{k_{-2}}{\overset{k_2}{\rightleftarrows}} C + D \tag{19}$$

implies the rate law

$$\frac{dC}{dt} = k_2[A][B] - k_{-2}[C][D] \tag{20}$$

1.7 Transition State Theory

Initiated by Wigner and Pilzer and extended by Eyring, transition state theory has become one of the most important theories in physical chemistry, which unveils the a

fundamental relation between the rate constant for a reaction and the enthalpy and entropy of activation for that reaction.

The essential assumption of transition state theory is that a quasi-equilibrium has been built up between the reactants and the activated complex at the saddle point. The rate is then directly proportional to the concentration of these complexes multiplied by the frequency ($\frac{k_B}{h}T$) with which they are converted into products.[14]

1.7.A Eyring equation

The derivation of Eyring equation can be illustrated through a bimolecular reaction as follows, and also can be generalized to unimolecular reactions.

$$A + B \xrightarrow{k} P \tag{21}$$

The objective is to compute the forward rate constant *k*. For the same bimolecular reaction sequence, transition state theory assumes that A and B reversibly react to form an intermediate complex $(AB)^{\ddagger}$, which irreversibly decomposes to form final product P. The species $(AB)^{\ddagger}$ is a so-called transition state (or a activated complex) whose lifetime is less than 10^{-13} sec. This can be shown schematically in Figure 1.

$$A + B \leftrightarrows [AB]^{\neq} \rightarrow P \tag{22}$$

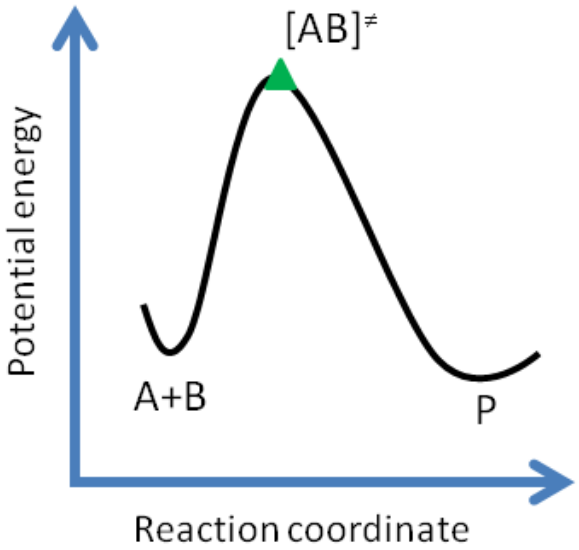

Figure 1. Potential energy diagram

The rate of product p formation is proportional to the concentration of the activated complex.

$$\frac{dP}{dt} = k[A][B] = k'[AB]^{\neq} \qquad (23)$$

where k is the bimolecular rate constant for the reaction of A and B to P and k' is the unimolecular rate constant for formation of product P from the activated complex $[AB]^{\neq}$ Under the transition state theory, there is a thermodynamic quasi-equilibrium existing between A, B and $[AB]^{\neq}$.

$$K^{\neq} = \frac{[\mathrm{AB}]^{\neq}}{[\mathrm{A}][\mathrm{B}]} \qquad (24)$$

So, the concentration of the transition state $[AB]^{\ddagger}$ is

$$[AB]^{\neq} = K^{\neq}[A][B] \tag{25}$$

Therefore the rate equation for the production of product is

$$\frac{dP}{dt} = k'[AB]^{\neq} = k^{\neq}K^{\neq}[A][B] = k[A][B] \tag{26}$$

where the rate constant k is given by

$$k = k^{\neq}K^{\neq} \tag{27}$$

During the activated complex formation, one bond is breaking while a vibration is being transformed into a translation as the bond breaks. $k^{\neq}$ is proportional to the frequency (ν) of the imaginary vibrational mode. A proportionality constant κ, also called transmission coefficient is introduced. So $k^{\neq}$ can be rewritten as

$$k^{\neq} = \kappa\nu \tag{28}$$

A temperature dependent expression of $K^{\ddagger}$ is brought from statistical mechanics as follows:

$$K^{\neq} = \frac{\kappa_B}{h\nu} T K^{\neq'} \quad (29)$$

where

$$K^{\neq'} = e^{\frac{-\Delta G^{\neq}}{RT}} \quad (30)$$

From above equations, the new rate constant expression can be re-written, which is given as

$$k = k^{\neq} K^{\neq} = \kappa \frac{k_B T}{h} e^{\frac{-\Delta G^{\neq}}{RT}} \quad (31)$$

The rate constant expression can be divided into two parts according to

$\Delta G = \Delta H - T\Delta S$. The final Eying equation is

$$k = \kappa \frac{k_B T}{h} e^{\frac{\Delta S^{\neq}}{R}} e^{\frac{-\Delta H^{\neq}}{RT}} \quad (32)$$

1.7.B Relation between theory and experiment

Experimentally two types of analysis are usually applied to measure the reaction physical quantities. Rate constants have been measured along a series of temperatures. The relationship between ln(k/T) versus 1/T can be plotted. The activation energy can be

readily obtained from this analysis during the range of data points. Application of the Arrhenius equation is an alternative choice.[4]

$$k = Ae^{-Ea/(RT)} \quad (33)$$

The Arrhenius activation energy is an important term that experimental scientists often refer to in the literature. It can be connected with calculated activation enthalpy as follows:[12]

$$E_a = \Delta H^{\neq} + RT - P\Delta V^{\neq} \quad (34)$$

where $\Delta V^{\neq}$ is the standard volume of activation. For a unimolecular reaction, from the reactions to the transition state, $\Delta V^{\neq}$ does not change. Thus,

$$E_a = \Delta H^{\neq} + RT \quad (35)$$

1.7.C Lindemann-Hinshelwood theory

Lindemann-Hinshelwood theory was first proposed by lindemann in 1922 which built up the basis for the modern theory of thermal unimolecular rates. The essential idea can be summarized as follows: the reaction molecules will be activated by bimolecular collisions first, which could then undergo deactivating collisions. One of the achievements of Lindemann-Hinshelwood theory is that it provides reasonable

explanations to the experimental observation that the reaction order is different at high- and low-pressure limit.

For example, the mechanism of the unimolecular reaction might be proposed:

$$X + M \overset{k_1}{\rightarrow} A^* + M \quad (36)$$

$$A^* + M \overset{k_{-1}}{\rightarrow} A + M \quad (37)$$

$$A^* \overset{k_2}{\rightarrow} \text{Products} \quad (38)$$

In this scheme, A^* represents the energized molecule and M is the third-body molecule, also called collision partner. Steady-state approximation is used to deduce the rate expression,

$$\text{rate} = k_{uni}[A] = k_2[A^*] = \frac{k_1 k_2 [A][M]}{k_{-1}[M] + k_2} \quad (39)$$

The high pressure and low pressure have been defined at $[M] \rightarrow \infty$ and $[M] \rightarrow 0$, respectively. Therefore, the high- and low-pressure rate constant expressions are

$$k_\infty = \frac{k_1 k_2}{k_{-1}} \quad (40)$$

and

$$k_0 = k_1[M]. \quad (41)$$

1.8 Variational Transition State Theory (VTST) and Generalized Transition State Theory

Transition state theory determines the reaction activation free energy from the activated complex based on the transition structure. TST can usually provide reasonable results for reactions with a tight reaction barrier, but it can not effectively handle reactions without a transition structure or with a loose transition state. Generalized transition state theory (GTST) was developed to deal with this deficiency of transition state theory.[15,16] The definition of GTST from IUPAC is "Any form of transition-state theory(TST), such as microcanonical variational TST, canonical variational TST, and improved canonical variational TST, in which the transition state is not necessarily located at the saddle point, is referred to as "generalized transition-state theory."[17] Variational transition state theory (VTST) is one of the common methods of GTST.

Conceptually, the procedure of VTST involves two steps. First the minimum-energy path (MEP) or the intrinsic reaction coordinate (IRC) is constructed. Second, the activation free energy will be calculated until the minimal rate constant is approached.

$$k^{VTST}(T,s) = min_s \frac{k_B}{h} T \frac{Q^{\neq}(TS)}{Q_R} \frac{Q_R^o}{Q^{\neq,o}} e^{-\Delta V^{\neq}(s)/k_B T} \qquad (42)$$

By definition, s = 0 is the position of the saddle point, and positive and negative values represent the product and reactant sides relative to the saddle point, respectively.

1.9 Variable Reaction Coordinate - Variational Transition State Theory (VRC-VTST)

The accurate calculation of rate constants for reactions without a barrier or with a loose barrier is always challenging, for instance, in the case of radical-radical associations. First of all, the dividing surface should be flexible and second, the calculated potential energy surfaces should be calculated with high-level electronic structure theory. For barrierless association reaction, the two reactants separated at infinite distance come to each other. The region beyond the transition-state region does not play a vital role since there is no interaction. In the transition-state region, free rotation modes of the individual reactants are gradually transformed into hindered rotations which are eventually converted into rigid bending vibrations. This significantly differs from the reactions with a tight barrier. The rigid-rotor harmonic-oscillator approximation can provide good results for tight barrier reaction. All orientations of the approaching fragments are crucial in the bond-forming range which is usually 1.5-6.0 Å.

In variable Reaction Coordinate - Variational Transition State Theory (VRC-VTST):[18,19] as it implies, a new reaction coordinate is proposed as follows in Figure 2.

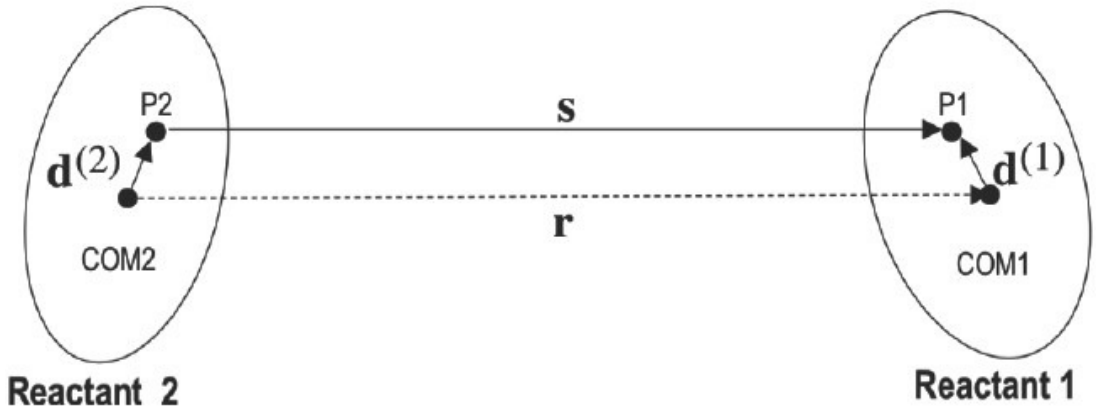

Figure 2. Schematic description of variable reaction coordinate.

The two ellipses represent reactant 1 and reactant 2, respectively. Center of mass is abbreviated as COM. P1 and P2 are pivot points associated with reactant 1 and reactant 2, respectively. Their positions vary according to different reactions. The vectors d(1) and d(2) are used to connect the pivots with their associated reactants center of mass (COM). The variable reaction coordinate is defined as distance of the vector connecting the two pivot points of the reactants. The distances will be fixed with a specified stepsize through the assigned distance range. All three vectors s, d(1), and d(2) will be sampled over the entire phase space simultaneously at fixed distances.

2.0 References:

(1) Jensen F. *Introduction to computational Chemsitry*, Wiley: New York, **1999.**

(2) Levine, I. N. *Quantum Chemistry, Fifth Ed.,* Prentice-Halll, Inc.; New Jersey, **2000.**

(3) Baer, M. *Beyond Born-Oppenheimer: Electronic non-Adiabatic Coupling Terms and Conical Intersections*, John Wiley & Sons, Inc.; Hoboken, N. J., Chapter 2, **2006.**

(4) Cramer, Christopher J. *Essentials of Computational Chemistry.* Chichester: John Wiley & Sons, Inc.; Hoboken, N. J., **2002.**

(5) Foresman, J. B.; Frisch, A. Exploring Chemistry with Electrnoic Structure Methods, 2nd Ed., Gaussian Inc. : Pittsburgh, 1996.

(6) Slater, J. C. *Phys. Rev.* **1930,** *36,* 57.

(7) Curtiss, L. A.; Redfern, P. C.; Raghavachari, K. *J. Chem. Phys.* **2007**, *126*, 084108.

(8) Curtiss, L. A.; Raghavachari, K.; Trucks, G. W.; Pople, J. A. *J. Chem. Phys.,* **1991,** *94,* 7221.

(9) Curtiss, L. A.; Raghavachari, K.; Trucks, G. W.; Pople, J. A. *J. Chem. Phys.,* **1998,** *109,* 7764.

(10) Petersson, G. A.; Bennett, A.; Tensfeldt, T. G.; Al-Laham, M. A.; Shirley, W. A., Mantzaris, J. *J. Chem. Phys.,* **1988,** *89,* 2193.

(11) Barnes, E. C.; Petersson, G. A.; Montgomery, J. A.; Frisch, M. J.; Martin, J. M. L. *J. Chem. Theory Comput.* **2009**, *5*, 2687.

(12) Steinfeld, J. I.; Francisco, J. S.; Hase, W. L.*; Chemical Kinetics and Dynamics, Second Ed.,* Prentice-Halll, Inc.; New Jersey, **1998.**

(13) Atkins, P. *Physical Chemistry, Sixth Ed.,* New York: Freeman, **1998.**

(14) Truhlar, D. G.; Garrett, B. C.; Klippenstein, S. J. *J. Phys. Chem.* **1996,** *100,* 12771.

(15) Truhlar, D. G.; Isaacson, A. D.; Garrett, B. C. In *Theory of Chemical Reaction Dynamics*; Baer, M., Ed.; CRC Press: Boca Raton, FL, 1985; p 65.

(16) Truhlar, D. G.; Garrett, B. C. *Acc. Chem. Res.* **1980**, *13*, 440.

(17) McNaught, A. D.; Wilkinson, A. *IUPAC. Compendium of Chemical Terminology, 2nd ed.* Oxford *:* Blackwell Scientific Publications, **1997.**

(18) Klippenstein, S. J. *J. Chem. Phys.* **1991**, *94*, 6469.

(19) Klippenstein, S. J. *J. Chem. Phys.* **1992**, *96*, 367.

Chapter 2

Computational Study of the Initial Stage of Diborane Pyrolysis

2.1 Introduction

The gas-phase pyrolysis of diborane is considered one of the most complicated processes in the entire field of chemistry.[1] Historically, pyrolysis of diborane has been used to prepare various polyboranes under different conditions.[2] Many experimental studies have been reported on the diborane pyrolysis and decomposition pathways, using such techniques as mass spectrometry,[3-6] chemical vapor deposition,[7-9] isotope exchange,[10-12] and gas chromatography.[13] Unfortunately, controversy surrounding the mechanism has not been resolved, even with the initial stage.[14-16] Generally, the first steps (eq 1 and eq 2a-c) are as follows:[15-18]

$$B_2H_6 \rightleftarrows 2\ BH_3 \qquad (1)$$

$$B_2H_6 + BH_3 \rightarrow B_3H_7 + H_2 \qquad (2a)$$

or

$$B_2H_6 + BH_3 \rightleftarrows B_3H_9 \qquad (2b)$$

$$B_3H_9 \rightleftarrows B_3H_7 + H_2 \qquad (2c)$$

$$2\ B_2H_6 \rightleftarrows B_3H_9 + BH_3 \qquad (3)$$

It is widely accepted that the symmetric dissociation of diborane initiates the pyrolysis.[19] However, several groups consider that the rate-determining step might be the

concerted formation and decomposition of B_3H_9 (eq 2a) or decomposition of B_3H_9 after its formation (eq 2b-c).[1,17,18] The most recent experiments carried out by Greatrex *et al.*[17] demonstrated that reaction 2a might be the rate-limiting step. An alternative mechanism initiated by reaction 3 was also proposed by Long *et al.*[20a] after an extensive systematic study of boron hydride reactions. This mechanism was also supported by Söderlund *et al.*[20b] It should be pointed out that reaction 3 has been largely ignored in the last decades. We suggest a reappraisal of the contribution of this step.

The 3/2 order dependence of the rate on the diborane concentration in the initial stage has been well established over the temperature range 373 to 550 K with an activation energy in the range of 22.0 - 29.0 kcal/mol (Table 1).[1,12b,13,14,17,21-26] This strongly implies that a triboron species is involved in the rate-limiting step.[18,21,22] Other important experimental observations include the inhibition by added H_2, which can also alter the product distribution.[14,21,22] Relative rates of pyrolysis of B_2H_6 and B_2D_6 were studied by mass spectrometry, from which a primary isotope effect k_H/k_D of 5.0 was determined,[18b] while a recent experimental reinvestigation yielded a smaller ratio of 2.57.[17] While previous kinetic studies have revealed additional details of this unusually complex reaction, in general, they support the above conclusions.[18,19]

The calculated activation energy can be matched with the observed barrier. For example, if reaction 1 is the initial step and reaction 2a is the rate-limiting step, the overall reaction activation energy can be expressed as eq 4 where the 1.5 RT term relates activation enthalpy to activation energy for a 3/2 order rate law (rate = $K_1^{1/2}k_{2a}[B_2H_6]^{3/2}$).

Table 1.Reaction activation energy (kcal/mol) of the pyrolysis of diborane

ΔE_a	Temperature (K)	Year	Ref
Exptl			
22.0±1.43	398-451	2000	23[b]
25.6	350-530	1993	26
24.5±0.8	393-453	1989	17
22.1±1.6	323-473	1987	14
10.1±0.3[a]	385-421	1973	25
29.0	343-473	1960	13
27.1±1.0	443-553	1960	23[a]
27.4	363-383	1951	21
25.5±0.5	373	1951	22
Calculation			
28.65(G4)	420	2013	this work
28.00(W1BD)	420	2013	this work
27.35[b]	420	2013	this work

a) The activation barrier was determined with a gas re-circulation device. It is not clear why the value is much lower than other results.

b) The enthalpy at 0 K of the $B_2H_6 \rightleftarrows 2\ BH_3$ reaction was taken from quantum Monte Carlo calculations in ref 62 and combined with G4 theory.

$$E_a = \Delta H^{\ddagger}_{overall} + 1.5RT = 0.5\Delta H_{rx1} + \Delta H^{\ddagger}_{2a} + 1.5RT \quad (4)$$

Two major difficulties are encountered in the experimental studies. First, the intermediates are difficult to identify due to their reactivity.[5,6] Second, because the experiments are generally carried out in a flask, the initial rates are difficult to isolate from competing secondary reactions.[3] A noteworthy exception was the study by Fernández *et al*.[25] where a gas recirculating technique was used to probe the initial rate.

Unfortunately, the exceptionally low activation barrier that was obtained for diborane pyrolysis (10.1 kcal/mol) suggests that there was some experimental difficulty.

On the theoretical side, uncertainty exists as to the structure of the intermediates. For example, two isomers of B_3H_9 have been proposed, a cyclic C_{3v} structure and a penta-coordinate C_2 butterfly structure.[27-34] In addition, at least two isomers of B_3H_7 have been proposed, a double-bridged form and a single-bridged form.[27-33] Due to the experimental difficulties of investigating the intermediate steps, high-level theoretical calculations may be the best tool to unravel the reaction mechanism. Over the last sixty years, quantum chemistry calculations have contributed to understanding the structures and reactivity of the boron hydrides.[15,16,29-36] In this work, we have investigated the possible mechanisms of the initial stage of diborane pyrolysis with high-level theory with the hope to shed light on the mechanism.

2.2 Computational methods

Frequencies and geometry optimizations for all boron hydrides involved in the reactions (Figure 1) were calculated using the G4 composite method.[37] The accuracy of the B3LYP/6-31G(2df,p) geometries (part of the G4 composite method) was checked by comparing with geometries on the minimum-energy pathway using the CCSD(T)[38-41] method with the 6-311G(d,p) basis set.[42,43] Stationary points in the low-lying pathways were also calculated by using the W1BD composite method.[44] Intrinsic reaction coordinate (IRC)[45] calculations were used to connect the reactant and product through a specific transition structure.

The minimum energy path (MEP) for the barrierless association of two boranes to form diborane has been determined by constrained optimization fixing the B-B distance to separations of 3.4 to 1.8 Å with a step size of 0.1 Å and optimizing all other variables. Single-point energy calculations at each geometry were made at the G4 level of theory. Vibrational frequencies along the reaction path were calculated after projecting out the reaction coordinate.

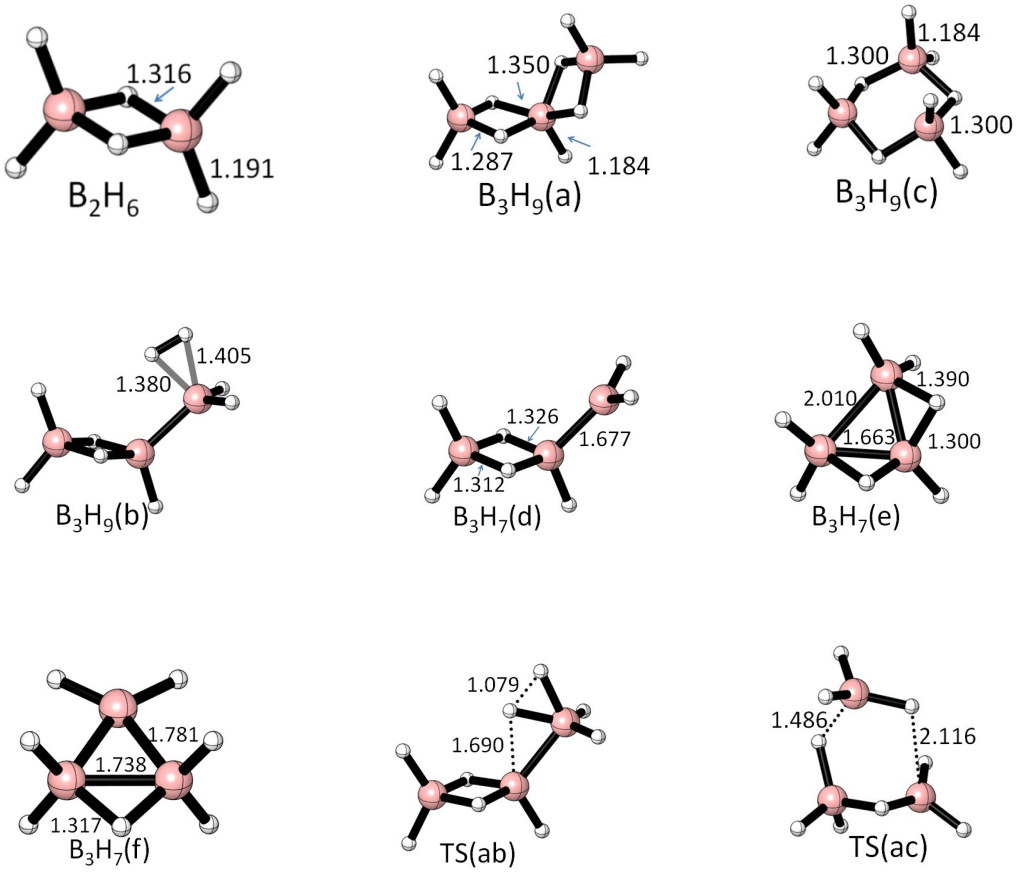

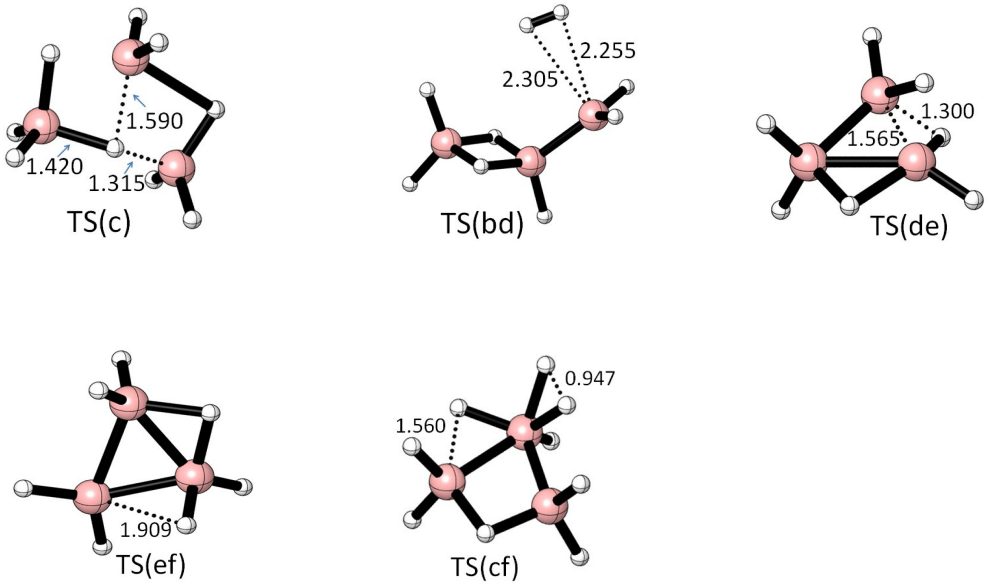

Figure 1. Optimized structures of the reactants, intermediates, and transition structures for the dissociation of B_2H_6 and the reaction of $BH_3 + B_2H_6$ at the G4 level. All the structures are also confirmed at the CCSD(T)/6-311G(d,p) level. All bond distances are in angstroms.

Equilibrium constants have been calculated from computed free energies ($K_p=\exp(-\Delta G^o/RT)$, where zero-point corrections, heat capacity corrections, and entropies have been included using standard techniques. All electronic structure calculations have been performed using the Gaussian 09 program suite.[46] The direct VRC[47,48]-VTST[49,50] method has been applied to calculate the rate constants of the barrierless association of BH_3 to diborane using the M06/MG3S and M06L/MG3S methods.[51,52] For the reaction $B_3H_9 \rightarrow B_3H_7+H_2$, which has a tight barrier, variational transition state theory with interpolated single-point energies (VTST[49,50]-ISPE[53], dual-level direct dynamics method) has been used to calculate the rate constants. Geometries and frequencies were generated

at the B3LYP/6-31G(2df,p) level of theory, while the reactants, transition structure, and products were re-determined with W1BD theory to improve the reaction energies. Rate constants were further corrected by zero-curvature tunneling (ZCT)[54] and small-curvature tunneling (SCT)[54] for tunneling effects.

Variable reaction coordinate - variational transition state theory (VRC-VTST) was used to investigate the kinetics of association of BH_3, which is very similar to the association of CH_3 radicals. Pivot points were fixed at 0.25 Å along the C_3 axis. A VRC reaction path was constructed by varying the distance between the pivot points in the range of 1.7 Å to 3.4 Å with a 0.1 Å step size. The VRC method avoids the difficulty of computing the inter-fragment modes where the transition from rotations in the reactants to vibrations in the product is very difficult to treat accurately. The M06/MG3S and M06L/MG3S methods were used because Truhlar and co-workers[55] found these methods to be accurate in the CH_3 association reaction. The rate constants have been calculated using Polyrate.[57] Gaussrate has been used as the interface between Gaussian 09 and Polyrate.[55] The natural bond orbital (NBO)[58] analysis was performed using the default NBO package in Gaussian 09.

2.3 Results and Discussion

The potential energy surface (including zero-point energy corrections) involving $B_2H_6 + BH_3$ was thoroughly explored at the G4 level (Figure 2). Good agreement is found with the transition structure (TS(c)) to form B_3H_9(c) and the transition structure (TS(cf)) to form B_3H_7(f)+ H_2 located at the G4 level and those reported by Lipscomb and co-workers[15] at the approximate MP2/6-31G(d) level. In particular, TS(c) features the

unusual triple-bridged hydrogen with B-H distances of 1.315, 1.420, and 1.590 Å. The calculated reaction enthalpies at 0 K from $B_2H_6 + BH_3$ to B_3H_9(c) and to B_3H_7(f) + H_2 agree to within about 3 kcal/mol of those reported by Lipscomb and co-workers[15] at the approximate CCSD(T)/6-31G(d)//MP2/6-31G(d) level. The significant difference between the two studies is the discovery of a new pathway through a penta-coordinate B_3H_9 intermediate with C_2 symmetry (B_3H_9(a)), which is less stable than B_3H_9(c) but is formed from $B_2H_6 + BH_3$ without an activation barrier. The activation enthalpy (0 K) for elimination of H_2 from B_3H_9(a) is 14.1 kcal/mol, larger than the barrier for loss of H_2 from B_3H_9(c) (11.7 kcal/mol). Through the B_3H_9(a) intermediate, elimination of H_2 has the larger barrier (14.1 kcal/mol), while through the B_3H_9(c) intermediate, formation from $B_2H_6 + BH_3$ has the larger barrier (13.5 kcal/mol). Duke *et al.*[27] have described the structure of B_3H_9(a), also known as the butterfly structure, and even predicted that the species could be important in the pyrolysis mechanism of diborane but they did not report any transition structures.

Both B_3H_9(a) and B_3H_9(c) lose H_2 to form a higher-energy isomer of B_3H_7 (B_3H_7(d) and B_3H_7(f), respectively). However, very small barriers exist for the rearrangement of both to the global minimum B_3H_7(e). From these steps, a mechanism can be postulated for the initial stage of diborane pyrolysis. The elementary step of this mechanism is the dissociation of diborane. Since the reverse reaction is the archetype for all fast boron hydride association reactions and since it has such elegant beauty, it deserves special treatment.

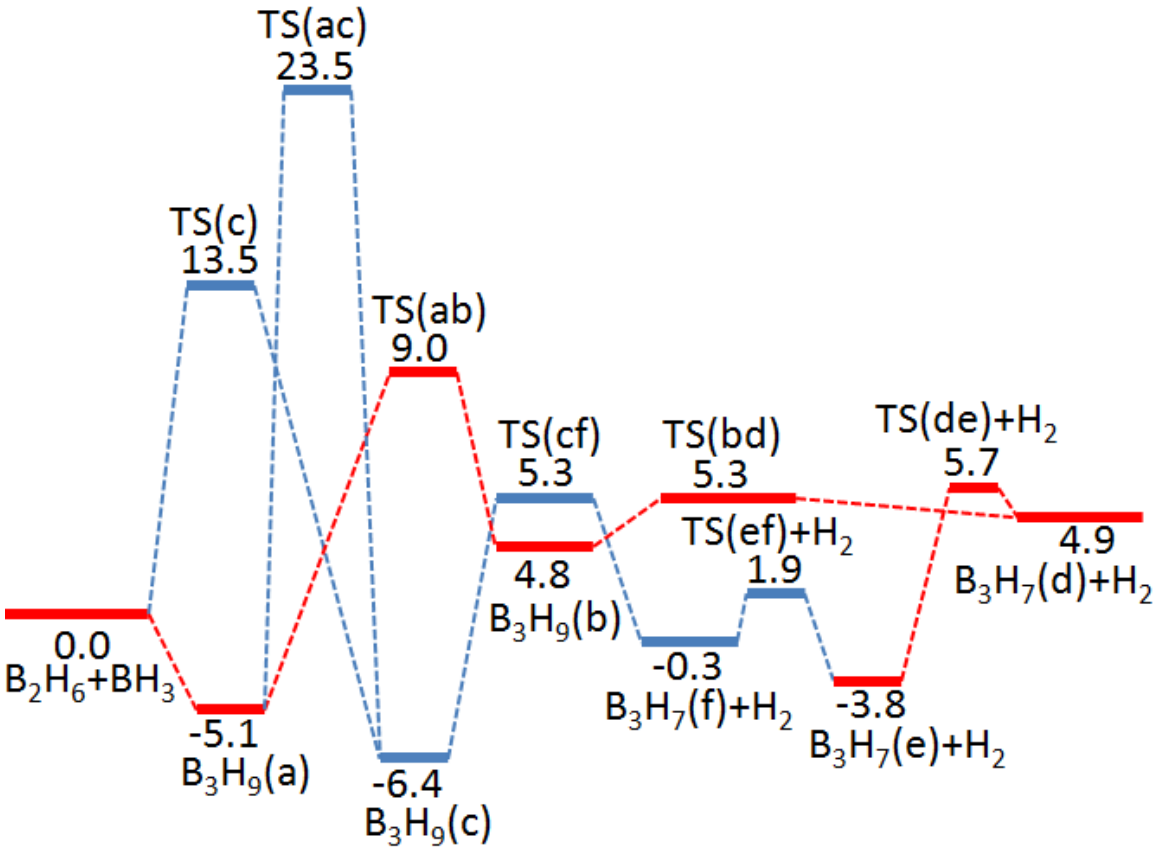

Figure 2. Schematic energy diagram of BH_3 + B_2H_6 at the G4 level of theory. The numbers represent the electronic energy plus zero point energy in kcal/mol.

2.3.A Association of BH_3

Although the reaction 2 $BH_3 \rightleftarrows B_2H_6$ is the inorganic version of the association of two methyl radicals to form ethane, it has not received nearly as much attention. The estimate of the rate constant at the high pressure limit for BH_3 association at 545 K is 6.6×10^{-11} $cm^3 \cdot molecule^{-1} \cdot s^{-1}$ which is about double the rate constant for CH_3 association at the same temperature (3.8×10^{-11} $cm^3 \cdot molecule^{-1} \cdot s^{-1}$).[59] This is unusual because the CH_3 association is more than twice as exothermic as the BH_3 association (90.8 kcal/mol versus 36±3 kcal/mol).[6,60,61] It is possible that the motion of the fragments at the bottleneck may

be more restricted in the CH_3 association reaction than in the BH_3 association which results in a smaller rate constant. However, the difference in rate constants may be within experimental uncertainty since the experimental rate constant for BH_3 association itself has a large uncertainty.[59]

To confirm the reliability of the level of theory, the symmetric dissociation energies of diborane using various methods have been collected in Table 2. They agree well with the experimental range of 36±3 kcal/mol as well as with the most accurate quantum Monte Carlo calculation (36.59 kcal/mol).[6,62] The equilibrium isotope effect for B_2H_6/B_2D_6 computed at the W1BD level at 400 K is $K_H/K_D = 2.0$, which is the same value as that reported by Lipscomb and co-workers.[16]

Since the association of BH_3 is barrierless, the reaction path was computed by reducing the B-B distance from 3.1 to 1.9 Å in steps of 0.1 Å (Figure 3). At each point along the reaction path, vibrational frequencies were computed by projecting out the transition vector. Free energies at 420 K were computed along the reaction path at the G4 level for B-B separations of 1.9 to 3.1 Å, in this range all of the projected vibrational frequencies are positive. The maximum on the free-energy curve occurs at R(B-B) = 2.9 Å where the free energy is 6.7 kcal/mol higher

Table 2.Thermochemistry (kcal/mol) for dissociation of diborane to two BH_3 Fragments

Level of theory	ΔE	Δ(E+ZPE)	ΔH(420K)	ΔG(420K)
W1BD	44.3	37.9	40.1	25.3
G4	43.6	37.2	39.5	24.6
M06L/MG3S[a]	46.6	42.1	42.1	27.3
CCSD(T)/6-311g(d,p)	42.8	34.1	36.4	21.5
CCSD(T)/6-311++g(3df,2p)	42.5	35.8	38.1	23.2
CCSD(T)/aug-cc-pVTZ	40.8	36.1	38.5	23.5
MP2/aug-cc-pVTZ	44.3	37.6	39.9	24.9

MP2/cc-PVTZ[b]	46.6	39.8	42.1	26.0
Diffuse Monte Carlo[c]	43.1	36.6		
Exptl[d]		36±3		

a) Scale factor for vibrational frequencies: 0.978.

b) Scale factor for vibrational frequencies: 0.95.

c) Ref 62.

d) Ref 6.

than that of the separated BH_3 fragments. At the B-B distance of 2.9 Å, the enthalpy is 2.6 kcal/mol lower than that for two BH_3 units, consistent with a barrierless reaction. The potential energy surface calculated by DeFrees *et al.*[63] at the MP2/6-31G(d) level of theory is in good agreement with our results.

NBO analysis, an effective tool to study donor-acceptor interactions, has been performed on points along the reaction surface at the MP2/aug-cc-pVTZ level of theory. Comparing second-order perturbative interaction values ($\Delta E^{(2)}$) within NBO theory allows the estimation of stabilization energies which represent the strength of the donor-acceptor interactions.[64] The $\Delta E^{(2)}$ of $\sigma_{B\text{-}H}$ from one BH_3 fragment to the n* orbital of the other BH_3 fragment at the free energy maximum (B-B = 2.9 Å) is 25.3 kcal/mol, while all other interactions are under 1 kcal/mol, indicating that the donor-acceptor interaction of $\sigma_{B\text{-}H}$ with n* is an important interaction in this association. Since the enthalpy at the free energy maximum is not much reduced from that of two boranes, other changes (such as the B-H bond distance) are destabilizing.

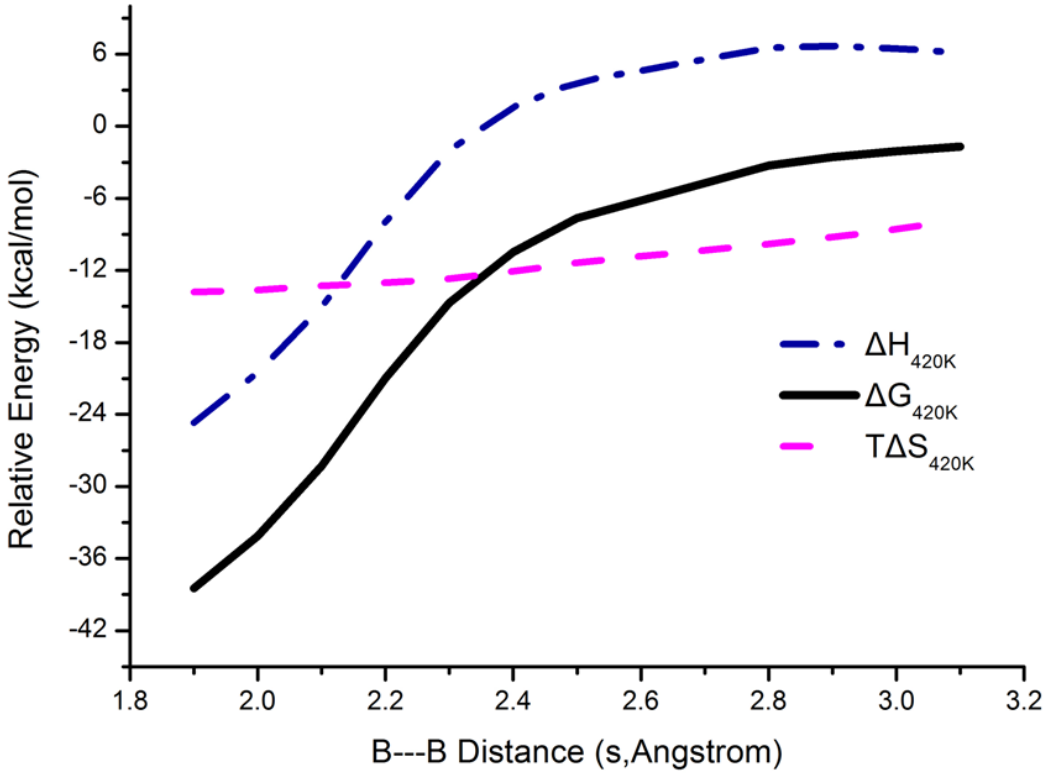

Figure 3. Reaction paths for dissociation of diborane. Quantities calculated at G4 level of theory are enthalpies, free energies, and entropy contributions to free energies. The sum of quantities of BH_3 and BH_3 at infinity distance have been taken as zero. The distance of extending B-B bond in diborane has been taken as the calibration for the reaction paths. The reaction coordinate has been projected out.

The symmetry of the reaction path for dissociation of diborane has been discussed previously.[59,63,65] Angle and bond length changes of diborane along the reaction path have been monitored in Figure 4. From 2.0 Å to 2.6 Å, the B3LYP/6-31G(2df,p), reaction path maintains C_{2h} symmetry. After 2.6 Å, the C_{2h} symmetry

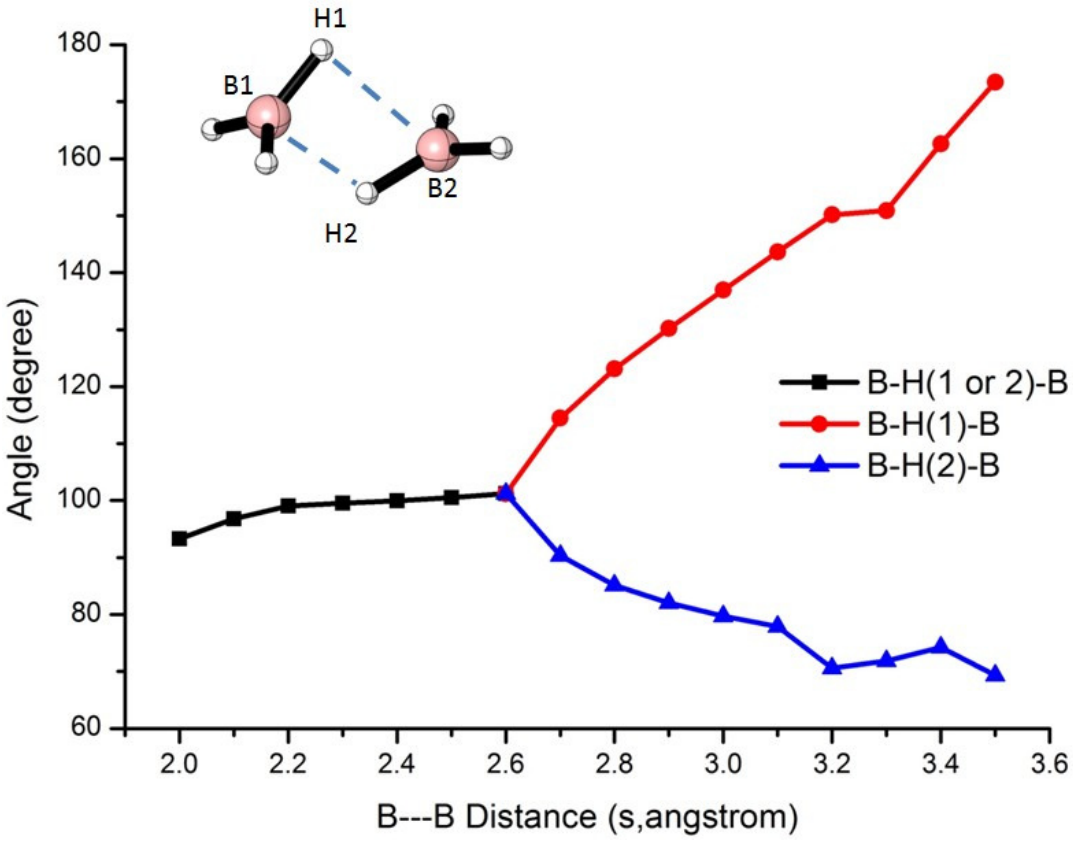

Figure 4. Comparison of two B-H(bridge)-B angle changes along the reaction coordinate.

All the geometries are optimized at the B3LYP/6-31G(2df,p) level of theory. is reduced to C_s where the B-H(1)-B and B-H(2)-B angles are unequal. Toinvestigate the origin of symmetry-breaking, NBO analysis was performed along the reaction path at the MP2/aug-cc-pVTZ level of theory (Figure 5). The sum of two unequal donor-acceptor interactions in the C_s-symmetry path are larger than the sum of two equal donor-acceptor interactions in the C_{2h}-symmetry path.

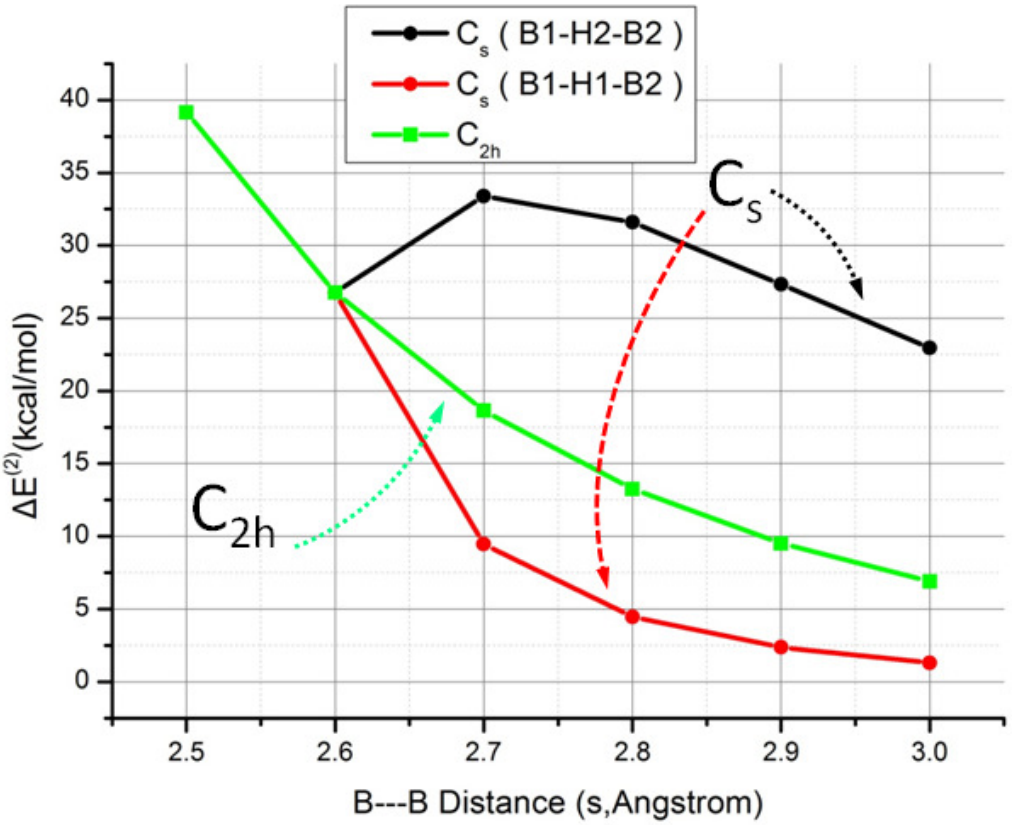

Figure 5. NBO 2nd order donor-acceptor stabilization energies for the reaction of BH_3 + BH_3 along the reaction path. C_s (B1-H2-B2) and C_s (B1-H1-B2) represent the $\sigma_{B\text{-}H} \rightarrow n^*$ interaction between H1 and B2, H2 and B1 respectively along the C_s reaction path. C_{2h} represents the $\sigma_{B\text{-}H} \rightarrow n^*$ interaction either H1-B2 or H2-B1 since they kept the same along the C_{2h} reaction path.

The high-pressure limit rate constants of association of BH_3 have been calculated at the M06/MG3S and M06L/MG3S levels of theory (Figure 6) rather than the dissociation rate constants of diborane because there were no direct experimental rate constants for the dissociation process. The dissociation rate constant of B_2H_6 (needed for the pyrolysis mechanism) can be easily obtained from the forward rate constant and the

equilibrium constant. The best experimental determination of the BH_3 association rate constant resulted from a study on the thermal decomposition of BH_3CO.[59] The experimental value corrected to the high pressure limit yielded a rate constant at 545 K of $10^{10.6\pm0.4}$ liter·mol^{-1}·s^{-1} or 6.6x10^{-11} cm^3·molecule^{-1}·s^{-1} in units used here. The calculated values evaluated at 550 K are 1.0x10^{-10}, 8.2x10^{-11}, and 1.6x10^{-10} cm^3·molecule^{-1}·s^{-1} at M06L/MG3S with VRC-VTST, M06/MG3S with VRC-VTST, and G4 with VTST, respectively.

2.3.B Pyrolysis of B_2H_6

2.3.B.1. Unimolecular Step as Initial Step (U path)

The present calculations of B_3H_9 and B_3H_7 isomers are in good agreement with previous studies.[15,16,28-36] In the search for the lowest-energy pathway, there has been discussion about whether the reaction proceeds as a two-step process with a B_3H_9 intermediate or as a single-step process, bypassing the B_3H_9 intermediate. The origin of the debate is that the calculated energy of the B_3H_9 C_{3v}-symmetry structure, when combined with one half of the B_2H_6 dissociation energy, leads to an activation barrier too large to be consistent with experiment.

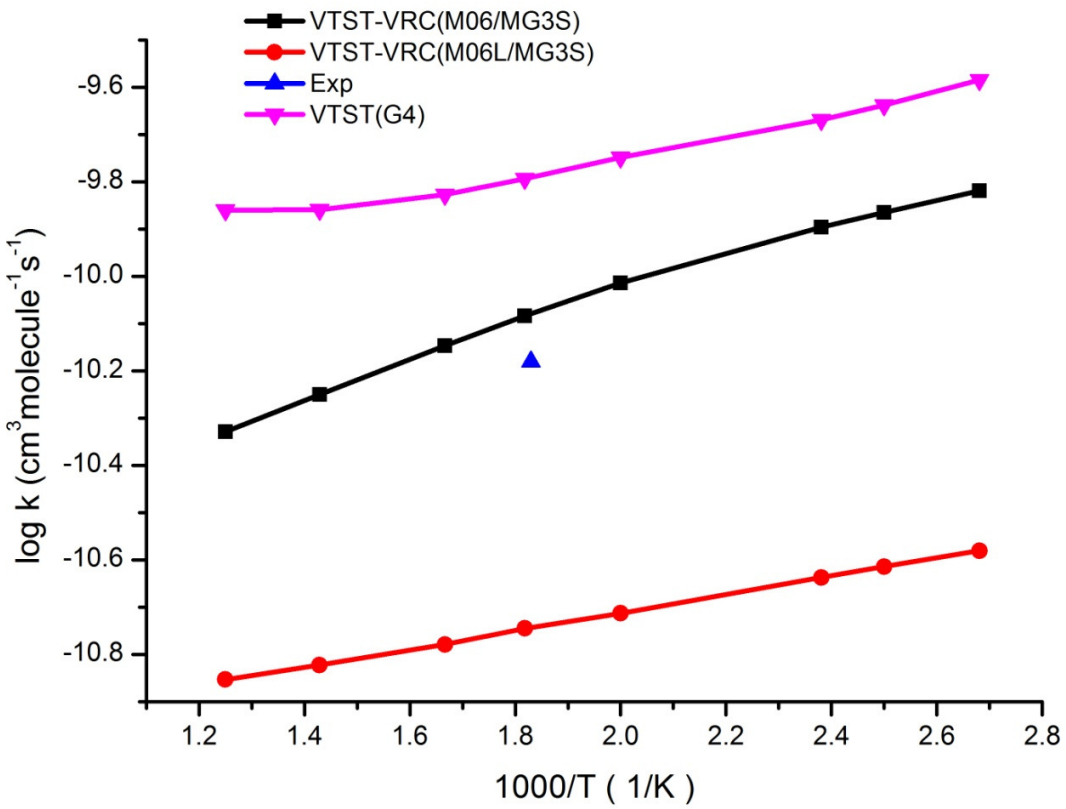

Figure 6. Calculated rate constants for the BH_3 association to B_2H_6.

The first step of the U path is the dissociation of diborane which was discussed in the previous section. The schematic enthalpy (0 K) diagram of the B_2H_6 + BH_3 reactions (Figure 2) is initiated with the barrierless reaction to form B_3H_9(a). The B_3H_9(c) species with C_{3v} symmetry is the most stable isomer of B_3H_9 but it is separated from B_2H_6 + BH_3 by a 13.5 kcal/mol barrier. While the penta-coordinate B_3H_9(a) with four bridging hydrogens and one terminal hydrogen is unknown, the butterfly structure of Al_3H_9 is known in the solid state.[66,67] In addition, a related butterfly structure of B_4H_{10} has been found to play a key role in its reactivity.[68]

From B_3H_9(a), there are two reaction paths; either the butterfly B_3H_9 can isomerize to B_3H_9(c) via a six-membered ring transition structure TS(ac) with an activation barrier of 28.6 kcal/mol followed by hydrogen release via TS(cf) to generate B_3H_7(f) + H_2, or pass over a 14.1 kcal/mol energy barrier via TS(ab). In the transition structure TS(ab), one terminal H atom and one bridging H atom from B_3H_9(a) form an H_2-B_3H_7 complex (B_3H_9(b)) which has a very small barrier for H_2 loss to form B_3H_7(f) + H_2. From the above PES (including zero-point corrections) of B_2H_6 + BH_3, it is apparent that TS(ab) is involved in the rate-limiting step. Since the addition of BH_3 to B_2H_6 forming B_3H_9(a) is a barrierless reaction, a reaction path was constructed where the B-B distance is decreased in 0.1 Å steps from 3.9 to 2.1 Å (Figure 7). To further explore the rate-limiting step, free energies at 420 K and other thermal properties of the reaction path are shown in Figure 7.

The butterfly B_3H_9(a) is a minimum on the PES (including zero-point corrections). While it is lower in enthalpy (ΔH_{420K}), it is higher in free energy (ΔG_{420K}) relative to B_2H_6 + BH_3. This suggests that B_3H_9(a) is only a minimum at low temperatures while at 420 K, B_3H_9(a) is a point on the reaction path toward B_3H_7(d) + H_2. Thus, the postulated concerted reaction between B_2H_6 + BH_3 $\rightarrow$ B_3H_7 + H_2 appears to be supported as shown by the free energy surface (420 K) in Figure 8. Except for a small bump when H_2 is lost from B_3H_7(d), the free energy surface at 420 K has the general shape of a concerted process. The free energy barrier is 20.8 kcal/mol and the overall reaction is spontaneous by 1.6 kcal/mol.

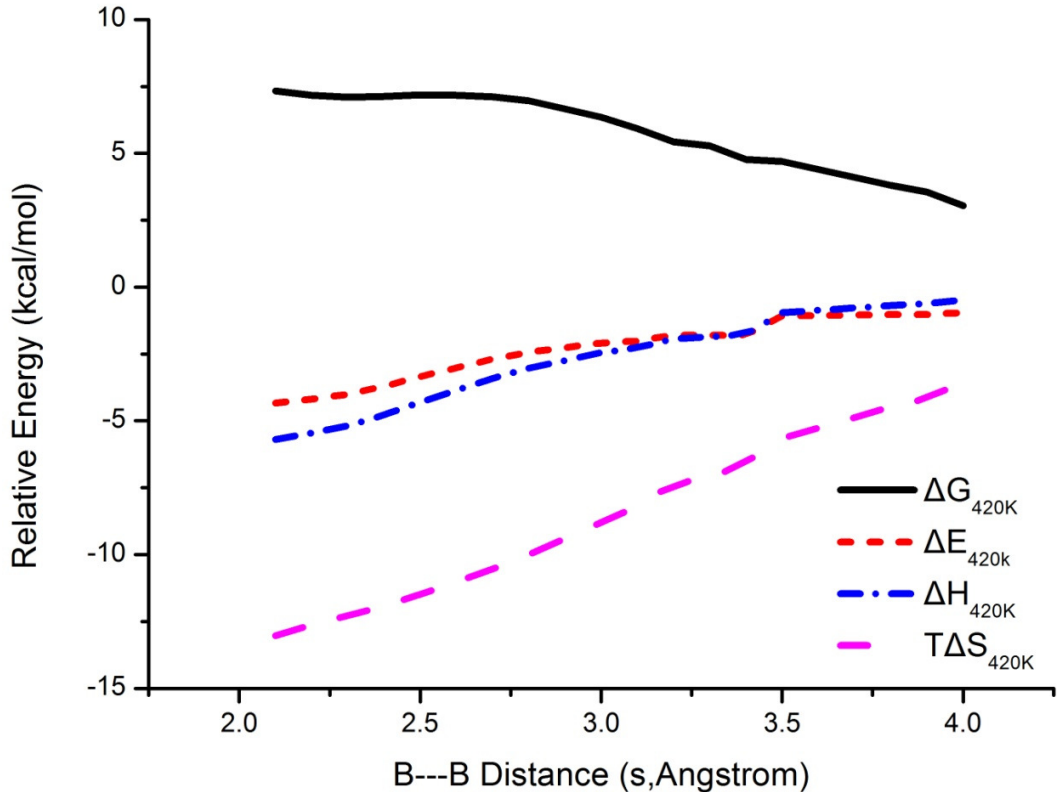

Figure 7. Reaction paths for $BH_3 + B_2H_6$. Quantities calculated at G4 level of theory are enthalpies, free energies, electronic energies plus zero-point vibrational energies (E_e + ZPE) and entropy contributions to free energies ($T\Delta S$). The sum of quantities of BH_3 and BH_3 at infinite distance have been taken as zero. The distance of the centered B and the terminal B atoms in diborane has been taken as the calibration for the reaction paths. Reaction coordinate has been projected out.

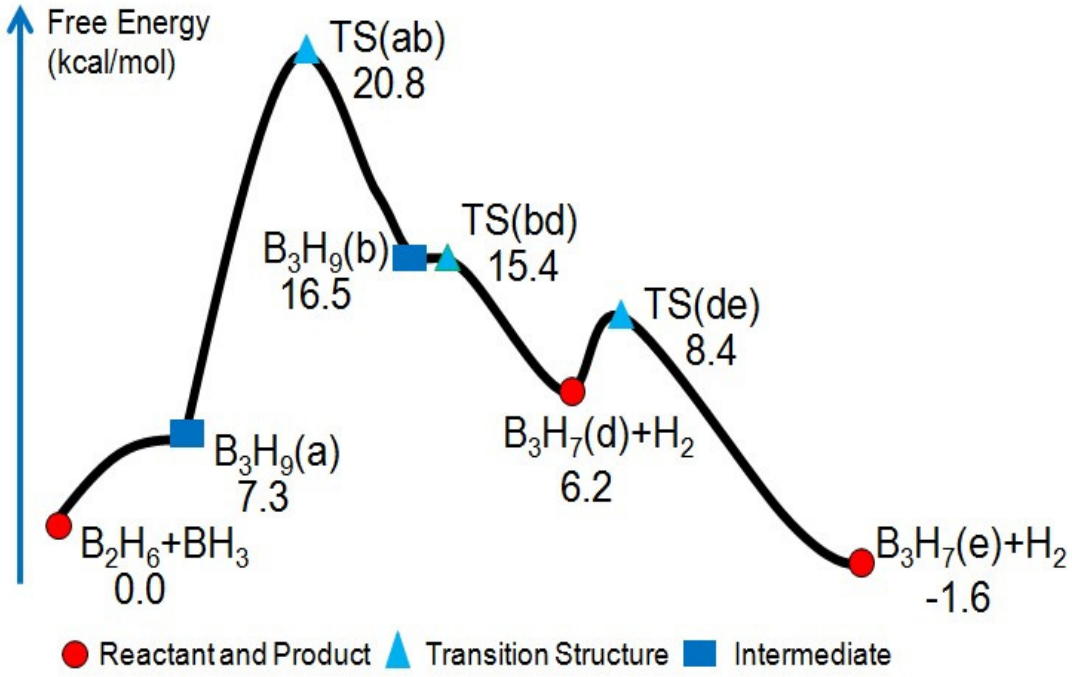

Figure 8. Free energy diagram in kcal/mol of BH_3 reaction with B_2H_6 at G4 level of theory (420 K).

2.3.B.2 Bimolecular Step as Initial Step (B path)

The pyrolysis can also start via a bimolecular reaction between two B_2H_6 molecules. At a first glance, entropy considerations would suggest that a bimolecular process could not compete with a unimolecular process except at very high B_2H_6 pressures. However, the products of the bimolecular reaction are B_3H_9 + BH_3 which already form a larger boron hydride. Thus, the first two steps of the "Unimolecular process" are unimolecular + bimolecular while the "Bimolecular process" are bimolecular + unimolecular. In the derivation of the two mechanistic variations, if the first two steps are considered as fast equilibria, the two variations generate the same rate law (see derivations 2.4 Rate law derivation).

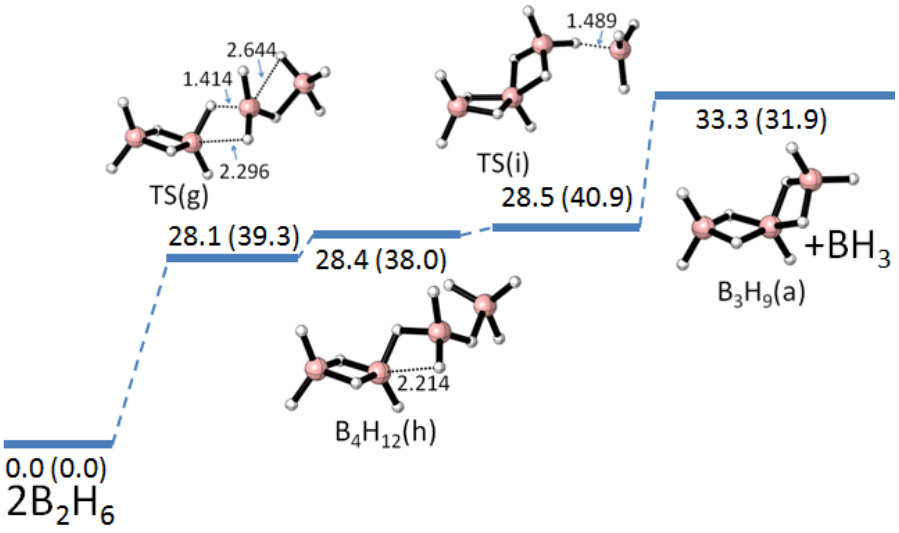

Figure 9. Enthalpy surface for the reaction of $B_2H_6 + B_2H_6 \rightarrow B_3H_9(a,C_2) + BH_3$. Enthalpies (kcal/mol) of $B_2H_6 + B_2H_6$ at 420 K are taken as zero. The values in parenthesis are free energies. Distances units are Angstroms.

Two bimolecular pathways have been calculated (Figures 9, 10). In the first (Figure 9), the products are $B_3H_9(a) + BH_3$ (path #1), while in the second (Figure 10), the products are $B_3H_9(c) + BH_3$ (path #2). The first step along the reaction path (path #1) involves the breaking of one hydrogen bridge and forming a new hydrogen bridge in the $B_3H_9(a)$-BH_3 complex ($B_4H_{12}(h)$) via transition structure TS(g). The product $B_3H_9(a)$-BH_3 complex decomposes to $B_3H_9(a)$ and BH_3 via transition structure TS(i). The complex $B_4H_{12}(h)$, transition structure TS(g) and TS(i) all have very similar enthalpies. One BH_4 structural unit in all three

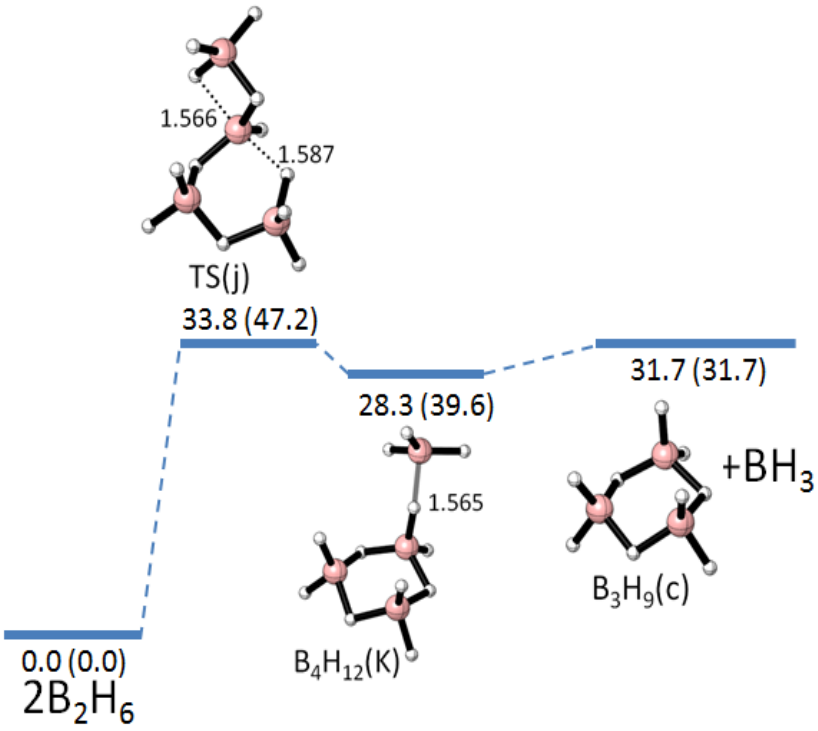

Figure 10. Enthalpy surface for the reaction of $B_2H_6 + B_2H_6 \rightarrow B_3H_9(c,C_{3v}) + BH_3$. Enthalpies (kcal/mol) of $B_2H_6 + B_2H_6$ at 420 K are taken as zero. The values in parenthesis are free energies. Distances units are Angstroms.

structures (intermediate and transition structures) is nearly static during the reaction. In the reaction path forming $B_3H_9(c)$ (path #2), the two B_2H_6 molecules unite to form a three-membered ring transition structure (TS(j)). The complex $B_4H_{12}(k)$ loses BH_3 spontaneously by 7.9 kcal/mol at 420 K.

The two pathways (#1 and #2) have free energy barriers (420 K) of 40.9 and 47.2 kcal/mol, respectively and are endothermic by 33.3 and 33.8 kcal/mol, respectively. Thus, pathway #1 forming $B_3H_9(a)$ is preferred. If the mechanistic derivation assumes fast equilibria for the initial two steps, then the equilibrium constant (not the rate

constant) enters the rate law. The following steps of the mechanism involve the reaction of the products (BH_3 and B_3H_9(a)). The BH_3 reacts with B_2H_6 as described above (eq 2b) while B_3H_9(a) decomposes to B_3H_7(d) + H_2 as described above (eq 2c).

2.3.B.3. General Discussion and Comparison with Experiment

From the above discussion, we propose two possible mechanistic variations. We name them as the Unimolecular (U path) and Bimolecular (B path) paths according to the initial step.

.

$$B_2H_6 \rightleftarrows 2\ BH_3 \quad k_{U1},\ k_{-U1},\ K_{U1} \qquad \text{(U1)}$$

$$B_2H_6 + BH_3 \rightleftarrows B_3H_7 + H_2 \quad k_{U2},\ k_{-U2},\ K_{U2} \qquad \text{(U2)}$$

$$B_2H_6 + B_3H_7 \rightarrow B_4H_{10} + BH_3 \quad k_{U3} \qquad \text{(U3)}$$

$$\text{Rate expression} = -\frac{d(B_2H_6)}{dt} = 2k_{U3}[B_2H_6]\frac{K_{U1}^{1/2}k_{U2}[B_2H_6]^{3/2}}{k_{-U2}[H_2] + k_{U3}[B_2H_6]} \qquad \text{(U4)}$$

$$\Delta E_a = \Delta H^{\ddagger}_{overall} + 1.5RT = 0.5\Delta H_{U1} + \Delta H^{\ddagger}_{U2} + 1.5RT \text{ when } k_{U3}[B_2H_6] >> k_{-U2}[H_2]$$

In the initial stage, $k_{U3}[B_2H_6] >> k_{-U2}[H_2]$, the right-hand side simplifies to $2K_{U1}^{1/2}k_{U2}[B_2H_6]^{3/2}$. The calculated activation energies (420 K) at the G4 and W1BD levels of theory are 28.65 and 28.00 kcal/mol, respectively. When the partial pressure of H_2 becomes significant, the rate of the pyrolysis is predicted to decrease which is consistent with experimental observations.[14] The overall pyrolysis rate constants

($k_{overall}$=$2K_{U1}^{1/2}k_{U2}$) calculated by various methods (Table 3) are smaller than experiment by three orders of magnitude. Deuterium isotope effects of k_H/k_D have also been explored in Table 4. Our results are in the range of a recent experiment at 420 K, but disagree with Enrione *et al.*[18b] at 361 K. Our calculated ratios are in satisfactory agreement with recent experimental results if experimental uncertainties are considered.[17]

Table 3. Rate constants ($cm^{3/2}\cdot molecule^{-1/2}\cdot s^{-1}$) of pyrolysis of B_2H_6 at 420 K[a,b]

	k_{u2}[d]				
K_{u1}[c]	CVT	TST/ZCT	CVT/ZCT	TST/SCT	CVT/SCT
W1BD	2.99E-14	2.23E-14	3.43E-14	2.38E-14	3.67E-14
G4	4.41E-14	3.30E-14	5.06E-14	3.53E-14	5.43E-14
M06L/MG3S	8.73E-15	6.49E-16	1.00E-14	6.98E-16	1.07E-14
MP2/cc-pVTZ	1.95E-14	1.45E-14	2.24E-14	1.56E-14	2.40E-14
Expt[e]			(1.86±0.36)E-11		

a) $k_{(overall)} = 2K_{U1}^{1/2}k_{U2}$.

b) The rate constant, k_{U2}, is computed with the VTST-ISPE method. The geometries at the reaction path were calculated at B3LYP/6-31G(2df,p) level. The higher-level electronic structure calculations at the W1BD level were used to correct the energies along the reaction path.

c) W1BD, G4, M06L/MG3S, and MP2/cc-pVTZ are the levels of theory used to calculate K_{U1}.

d) CVT, TST/ZCT, CVT/ZCT, TST/SCT, and CVT/SCT are the methods used to correct the rate constants in eq U2 for tunneling effects (see Polyrate manual).

e) Ref 16.

Table 4. Ratio of rate constants (k_H/k_D) for the pyrolysis of B_2H_6/B_2D_6 at 420 K[a-d]

	CVT	TST/ZCT	CVT/ZCT	TST/SCT	CVT/SCT
W1BD	2.25	1.54	1.83	1.60	3.75
G4	2.22	1.53	1.82	1.59	3.70
M06L/MG3S	2.34	1.61	1.93	1.68	3.90
MP2/cc-pVTZ	1.94	1.34	1.60	1.39	3.26
Exp			1.92-3.22[e] ≈5[f]		

a) $k_{(overall)} = 2K_{U1}^{1/2}k_{U2}$.

b) The rate constant, k_{U2}, is computed with the VTST-ISPE method. The geometries at the reaction path were calculated at B3LYP/6-31G(2df,p) level. The higher-level electronic structure calculations at W1BD level were used to correct the energies along the reaction path.

c) W1BD, G4, M06L/MG3S and MP2/cc-pVTZ are the levels of theory used to calculate K_{U1}.

d) CVT, TST/ZCT, CVT/ZCT, TST/SCT, and CVT/SCT are the methods used to correct the rate constants in eq U2 for tunneling effects (see Polyrate manual).

e) Ref 17.

f) Ref 18b.

In the B path the steady-state approximation was employed along with the sum of reaction B1 and -B2 (gives $B_2H_6 \rightleftarrows 2\ BH_3$) to derive a mechanistic rate law. The B path was proposed originally by Long *et al.*[20a] who made a careful analysis of previous experiment work.

$2\ B_2H_6 \rightleftarrows BH_3 + B_3H_9(a)$ k_{B1}, k_{-B1}, K_{B1} (B1)

$BH_3 + B_2H_6 \rightleftarrows B_3H_9(a)$ k_{B2}, k_{-B2}, K_{B2} (B2)

$B_3H_9(a) \rightarrow B_3H_7 + H_2$ k_{B3} (B3)

$B_2H_6 + B_3H_7 \rightarrow B_4H_{10} + BH_3$ k_{U3} (U3)

$$\text{Rate expression} = -\frac{d(B_2H_6)}{dt} = 2K_{B1}{}^{1/2}K_{B2}{}^{1/2}k_{B3}[B_2H_6]^{3/2} \quad \text{(B4)}$$

$$\Delta E_a = \Delta H^{\ddagger}_{overall} + 1.5RT = \Delta H_{B1} + \Delta H_{B2} + \Delta H^{\ddagger}_{B3} + 1.5RT$$

The calculated reaction activation energy is 28.65 kcal/mol, the same as the U path at 420 K at the same level of theory.

The rate of consumption of diborane can be accelerated through diborane scavenging reactions such as reaction U3. As the reaction proceeds, many additional reactive intermediates are formed which can also react with B_2H_6. Thus, additional reactions will deplete B_2H_6 in competition with the initial reactions and may have the overall effect of reducing the effective activation barrier and increasing the consumption rate of diborane.

2.4 Rate law deviation

2.4.A. U Path

$B_2H_6 \rightleftarrows 2\ BH_3$ k_{U1}, k_{-U1}, K_{U1} (U1)

$B_2H_6 + BH_3 \rightleftarrows B_3H_7 + H_2$ k_{U2}, k_{-U2}, K_{U2} (U2)

$B_2H_6 + B_3H_7 \rightarrow B_4H_{10} + BH_3$ k_{U3} (U3)

Steady state approximation:

$$\frac{d(B_2H_6)}{dt} = -k_{U1}[B_2H_6]-k_{U2}[B_2H_6][BH_3]+k_{-U2}[B_3H_7][H_2]-k_{U3}[B_2H_6][B_3H_7]+$$

$k_{-U1}[BH_3]$ (a)

$$\frac{d(BH_3)}{dt} = 2k_{U1}[B_2H_6]-k_{U2}[B_2H_6][BH_3]+k_{-U2}[B_3H_7][H_2]+k_{U3}[B_2H_6][B_3H_7]-$$

$2k_{-U1}[BH_3]^2 = 0$ (b)

$$\frac{d(B_3H_7)}{dt} = k_{U2}[B_2H_6][BH_3]-k_{-U2}[B_3H_7][H_2]-k_{U3}[B_2H_6][B_3H_7] = 0$$ (c)

Equation (b) + (c),

$k_{U1}[B_2H_6] = k_{-U1}[BH_3]^2$, $[BH_3] = (K_{U1}[B_2H_6])^{1/2}$ (e)

Equation (a) + (c),

$$\frac{d(B_2H_6)}{dt} = -2k_{U3}[B_2H_6][B_3H_7]$$ (f)

from equation (c),

$$[B_3H_7] = \frac{k_{U2}[B_2H_6][BH_3]}{k_{-U2}[H_2]+k_{U3}[B_2H_6]}$$ (g)

Therefore, rate expression $= -\frac{d(B_2H_6)}{dt} = 2k_{U3}[B_2H_6]\frac{K_{U1}^{1/2}k_{U2}[B_2H_6]^{3/2}}{k_{-U2}[H_2]+k_{U3}[B_2H_6]}$ (h)

2.4.B B Path

$2\ B_2H_6 \rightleftarrows B_3H_9(a) + BH_3$ k_{B1}, k_{-B1}, K_{B1} (B1)

$B_2H_6 + BH_3 \rightleftarrows B_3H_9(a)$ k_{B2}, k_{-B2}, K_{B2} (B2)

$B_3H_9(a) \rightarrow B_3H_7 + H_2$ k_{B3} (B3)

$B_2H_6 + B_3H_7 \rightarrow B_4H_{10} + BH_3$ $\quad k_{U3}$ (U3)

Steady state approximation:

$$\frac{d(B_2H_6)}{dt} = -2k_{B1}[B_2H_6]^2+2k_{-B1}[B_3H_9(a)][BH_3]-k_{B2}[B_2H_6][BH_3]+k_{-B2}[B_3H_9(a)]-$$

$k_{U3}[B_2H_6][B_3H_7]$ (i)

$$\frac{d(BH_3)}{dt} = k_{B1}[B_2H_6]^2-k_{-B1}[B_3H_9(a)][BH_3]-k_{B2}[B_2H_6][BH_3]+k_{-}$$

$_{B2}[B_3H_9(a)]+k_{U3}[B_2H_6][B_3H_7] = 0$ (j)

$$\frac{d(B_3H_7)}{dt} = k_{B3}[B_3H_9(a)]-k_{U3}[B_3H_7][B_2H_6] = 0$$ (k)

Equation (h) ~ (i),

$$\frac{d(B_2H_6)}{dt} = -3k_{B1}[B_2H_6]^2+3k_{-B1}[B_3H_9(a)][BH_3]-2k_{U3}[B_2H_6][B_3H_7]$$ (l)

Since reaction (B1) and (B2) have been assumed to be in fast equilibrium,

$k_{B3} << k_{-B2}$, $k_{U3} << k_{-B2}$

$k_{B1}[B_2H_6]^2-k_{-B1}[B_3H_9(a)][BH_3] \approx 0$ (m)

$[B_3H_9(a)]-K_{B2}[B_2H_6][BH_3] \approx 0$ (n)

From equation (m) and (n)

$[BH_3]^2-K_{B1}K_{B2}^{-1}[B_2H_6] \approx 0$ (o)

Therefore, $-\frac{d(B_2H_6)}{dt} = 2k_{U3}[B_2H_6][B_3H_7] = 2k_{B3}[B_3H_9(a)]$ (r)

Put (n) and (m) into (r),

rate expression $= -\frac{d(B_2H_6)}{dt} = 2K_{B1}^{1/2}K_{B2}^{1/2}k_{B3}[B_2H_6]^{3/2}$ (s)

2.5 Conclusion

The gas-phase kinetics of the initial stage of diborane pyrolysis has been probed at different levels of theory with variational transition state theory (VTST). The B_3H_9 isomer with C_{3v} symmetry does not play a role in the pyrolysis mechanism. Instead, a novel B_3H_9 butterfly structure with C_2 symmetry is on the free energy surface between $B_2H_6 + BH_3$ and $B_3H_7 + H_2$. The overall activation barrier is 28.65 kcal/mol at the G4 level. Two reaction variations have been proposed to elucidate the pyrolysis of diborane (U and B paths) which differ by the initial reaction step (unimolecular or bimolecular). Both variations reduce to the same rate law if the initial steps are assumed to be in fast equilibrium. Our long-term goal is to unravel the entire process to the formation of $B_{10}H_{14}$.

2.6 References:

(1) Greenwood, N. N. *Chem. Soc. Rev.* **1992**, *21*, 49.

(2) Stock, A. *The Hydrides of Boron and Silicon*, Cornell University Press: New York, 1933.

(3) Baylis, A. B.; Pressley, G. A.; Stafford, F. E. *J. Am. Chem. Soc.* **1966**, *88*, 2428.

(4) Stafford F. E.; Pressley G. A.; Baylis A. B. In *Mass Spectrometry in Inorganic Chemistry*; American Chemical Society: 1968; Vol. 72, p 137.

(5) Fehlner, T. P.; Fridmann, S. A. *Inorg. Chem.* **1970**, *9*, 2288.

(6) Fehlner, T. P.; Mappes, G. W. *J. Chem. Phys.* **1969,** *73,* 873.

(7) Rayar, M.; Supiot, P.; Veis, P.; Gicquel, A. *J. Appl. Phys.* **2008,** *104*, 033304.

(8) Mehta, B.; Tao, M. *J. Electrochem. Soc.* **2005**, *152*, G309.

(9) Mohammadi, V.; de Boer, W. B.; Nanver, L. K. *Appl. Phys. Lett.* **2012,** *101,* 111906.

(10) Rigden, J. S.; Koski, W. S. *J. Am. Chem. Soc.* **1961,** *83,* 552.

(11) Maybury, P. C.; Koski, W. S. *J. Chem. Phys.* **1953,** *21,* 742.

(12) (a) Todd, J. E.; Koski, W. S. *J. Am. Chem. Soc.* **1959,** *81,* 2319. (b) Koski, W. S. In *Borax to Boranes*, American Chemical Society, Washington, D.C.: 1961; Vol 32, p 78-87.

(13) Borer, K.; Littlewood, A. B.; Phillips, C. S. G. *Inorg. Nucl. Chem.* **1960**, *15*, 316.

(14) Greenwood, N. N.; Greatrex, R. *Pure Appl. Chem.* **1987**, *59*, 857.

(15) Stanton, J. F.; Lipscomb, W. N.; Bartlett, R. J. *J. Am. Chem. Soc.* **1989**, *111*, 5165.

(16) Lipscomb, W. N.; Stanton, J. F.; Connick, W. B.; Magers, D. H. *Pure Appl. Chem.* **1991**, *63*, 335.

(17) Greatrex, R.; Greenwood, N. N.; Lucas, S. M. *J. Am. Chem. Soc.* **1989**, *111*, 8721.

(18) (a) A brief summary of early kinetic studies of diborane pyrolysis is provided in the following: *Production of the Boranes and Related Research,* Holzmann, R. T., Ed.; Academic Press: New York, 1967; pp 90-115. (b) Enrione, R. E.; Schaeffer, R. J. *Inorg. Nucl. Chem.* **1961**, *15,* 103.

(19) Fehlner, T. P. In *Boron Hydride Chemistry;* Muetterties, E. L.,Ed.; Academic Press: New York, 1975 and references cited therein.

(20) (a) Long, L. H. *J. Inorg. Nucl. Chem.* **1970,** *32,* 1097. (b) Söderlund, M.; Mäki-Arvela, P.; Eränen, K.; Salmi, T.; Rahkola, R.; Murzin, D. Y. *Catal. Lett.* **2005,** *105,* 191.

(21) Clarke, R. P.; Pease, R. N. *J. Am. Chem. Soc.* **1951**, *73*, 2132.

(22) Bragg, J. K.; Mccarty, L. V.; Norton, F. J. *J. Am. Chem. Soc.* **1951**, *73*, 2134.

(23) (a) Owen, A. J. *J. Appl. Chem.* **1960**, *10*, 483. (b) Attwood, M. D.; Greatrex, R.; Greenwood, N. N.; Potter, C. D. *J. Organomet. Chem.* **2000**, *614*, 144.

(24) McCarty, L. V.; Giorgio, P. A. D. *J. Am. Chem. Soc.* **1951,** *73,* 3138.

(25) Fernández, H.; Grotewold, J.; Previtali, C. *M. J. Chem. Soc. Dalton Trans.* **1973,** 2090.

(26) Colket, M. B.; Montgomery, J. A. J. *Presentation to the Joint Technical Meeting of the Eastern States and Central States of the Combustion Institute*, New Orleans, LA 1993.

(27) Duke, B. J.; Gauld, J. W.; Schaefer, H. F. *J. Am. Chem. Soc.* **1995**, *117*, 7753.

(28) Stanton, J. F.; Lipscomb, W. N.; Bartlett, R. J.; Mckee, M. L. *Inorg. Chem.* **1989**, *28*, 109.

(29) Stanton, J. F.; Bartlett, R. J.; Lipscomb, W. N. *Chem. Phys. Lett.* **1987,** *138,* 525.

(30) Olson, J. K.; Boldyrev, A. I. *Inorg. Chem.* **2009**, *48*, 10060.

(31) Mckee, M. L. *J. Phys. Chem.* **1990**, *94*, 435.

(32) McKee, M. L. *J. Am. Chem. Soc.* **1990**, *112*, 6753.

(33) Tian, S. X. *J. Phys. Chem. A* **2005**, *109*, 5471.

(34) Duke, B. J.; Liang, C. X.; Schaefer, H. F. *J. Am. Chem. Soc.* **1991**, *113*, 2884.

(35) Olah, G. A.; Surya Prakash, G. K.; Rasul, G. *Proc. Natl. Acad. Sci. USA.* **2012,** *109,* 6825.

(36) Yao, Y.; Hoffmann, R. *J. Am. Chem. Soc.* **2011,** *133,* 21002.

(37) Curtiss, L. A.; Redfern, P. C.; Raghavachari, K. *J. Chem. Phys.* **2007**, *126*, 084108.

(38) Purvis, G. D., III; Bartlett, R. J. *J. Chem. Phys.* **1982,** *76,* 1910.

(39) Raghavachari, K.; Trucks, G. W.; Pople, J. A.; Head-Gordon, M. *Chem. Phys. Lett.* **1989,** *157,* 479.

(40) Watts, J. D.; Gauss, J.; Bartlett, R. J. *J. Chem. Phys.* **1993,** *98,* 8718.

(41) Bartlett, R. J.; Musial, M. *Rev. Mod. Phys.* **2007,** *79,* 291.

(42) Ditchfield, R.; Hehre, W. J.; Pople, J. A. *J. Chem. Phys.* **1972,** *56,* 2257.

(43) Krishnan, R.; Binkley, J. S.; Seeger, R.; Pople, J. A. *J. Chem. Phys.* **1980,** *72,* 650.

(44) Barnes, E. C.; Petersson, G. A.; Montgomery, J. A.; Frisch, M. J.; Martin, J. M. L. *J. Chem. Theory Comput.* **2009**, *5*, 2687.

(45) Fukui, K. *Acc. Chem. Res.* **1981**, *14*, 363.

(46) Frisch, M. J.; Trucks, G. W.; Schlegel, H. B.; Scuseria, G. E.; Robb, M. A.; Cheeseman, J. R.; Montgomery, Jr., J. A.; Vreven, T.; Kudin, K. N.; Burant, J. C.; Millam, J. M.; Iyengar, S. S.; Tomasi, J.; Barone, V.; Mennucci, B.; Cossi, M.; Scalmani, G.; Rega, N.; Petersson, G. A.; Nakatsuji, H.; Hada, M.; Ehara, M.; Toyota, K.; Fukuda, R.; Hasegawa, J.; Ishida, M.; Nakajima, T.; Honda, Y.; Kitao, O.; Nakai, H.; Klene, M.; Li, X.; Knox, J. E.; Hratchian, H. P.; Cross, J. B.; Bakken, V.; Adamo, C.; Jaramillo, J.; Gomperts, R.; Stratmann, R. E.; Yazyev, O.; Austin, A. J.; Cammi, R.; Pomelli, C.; Ochterski, J. W.; Ayala, P. Y.; Morokuma, K.; Voth, G. A.; Salvador, P.; Dannenberg, J. J.,; Zakrzewski, V. G.; Dapprich, S.; Daniels, A. D.; Strain, M. C.; Farkas, O.; Malick, D. K.; Rabuck, A. D.; Raghavachari, K.; Foresman, J. B.; Ortiz, J. V.; Cui, Q.; Baboul, A. G.; Clifford, S.; Cioslowski, J.; Stefanov, B. B.; Liu, G.; Liashenko, A.; Piskorz, P.; Komaromi, I.; Martin, R. L.; Fox, D. J.; Keith, T.; Al-Laham, M. A.; Peng, C. Y.; Nanayakkara, A.; Challacombe, M.; Gill, P. M. W.; Johnson, B.; Chen, W.; Wong, M. W.; Gonzalez, C.; Pople, J. A., *Gaussian09***;** Gaussian Inc.: Pittsburgh, PA, **2009**.

(47) Klippenstein, S. J. *J. Chem. Phys.* **1991**, *94*, 6469.

(48) Klippenstein, S. J. *J. Chem. Phys.* **1992**, *96*, 367.

(49) Truhlar, D. G.; Isaacson, A. D.; Garrett, B. C. In *Theory of Chemical Reaction Dynamics*; Baer, M., Ed.; CRC Press: Boca Raton, FL, 1985; Vol 4, p 65-137.

(50) Truhlar, D. G.; Garrett, B. C. *Acc. Chem. Res.* **1980**, *13*, 440.

(51) Zhao, Y.; Truhlar, D. G. *Theor. Chem. Acc.* **2008**, *120*, 215.

(52) Zhao, Y.; Truhlar, D. G. *Acc. Chem. Res.* **2008**, *41*, 157.

(53) Chuang, Y.-Y.; Corchado, J. C.; Truhlar, D. G. *J. Phys. Chem. A.* **1999**, *103*, 1140.

(54) Chuang, Y.-Y.; Truhlar, D. G. *J. Phys. Chem. A* **1997**, *101*, 3808.

(55) Zheng, J.; Zhang, S. X.; Truhlar, D. G. *J. Phys. Chem. A* **2008**, *112*, 11509.

(56) Zheng, J., *et al.* Polyrate 2010-A; University of Minnesota: Minneapolis, MN, **2010**.

(57) Zheng, J.; Zhang, S.; Corchado, J. C.; Chuang, Y.-Y.; Coitiño, E. L.; Ellingson, B. A.; Truhlar, D. G. Gaussrate 2009-A; University of Minnesota: Minneapolis, MN, **2010**.

(58) Glendening, E. D.; Reed, A. E.; Carpenter, J. E.; Weinhold, F. *NBO Version 3.1.*

(59) Mappes, G. W.; Fridmann, S. A.; Fehlner, T. P. *J. Phys. Chem.* **1970**, *74*, 3307.

(60) Baulch, D. L.; Cobos, C. J.; Cox, R. A.; Esser, C.; Frank, P.; Just, T.; Kerr, J. A.; Pilling, M. J.; Troe, J.; Walker, R. W.; Warnatz, J. *J. Phys. Chem. Ref. Data.* **1992,** *21,* 411.

(61) Baulch, D. L.; Cobos, C. J.; Cox, R. A.; Frank, P.; Hayman, G.; Just, T.; Kerr, J. A.; Murrells, T.; Pilling, M. J.; Troe, J.; Walker, R. W.; Warnatz, J. *J. Phys. Chem. Ref. Data.* **1994,** *23,* 847.

(62) Fracchia, F.; Bressanini, D.; Morosi, G. *J. Chem. Phys.* **2011**, *135*, 094503.

(63) Defrees, D. J.; Raghavachari, K.; Schlegel, H. B.; Pople, J. A.; Schleyer, P. v. R. *J. Phys. Chem.* **1987**, *91*, 1857.

(64) Reed, A. E.; Curtiss, L. A.; Weinhold, F. *Chem. Rev.* **1988**, *88*, 899.

(65) Dixon, D. A.; Pepperberg, I. M.; Lipscomb, W. N. *J. Am. Chem. Soc.* **1974,** *96,* 1325.

(66) Duke, B. J.; Gauld, J. W.; Schaefer, H. F. *Chem. Phys. Lett.* **1991,** *230,* 306.

(67) Nold, C. P.; Head, J. D. *J. Phys. Chem. A* **2012,** *116,* 4348.

(68) (a) McKee, M. L. *Inorg. Chem.* **1986**, *25*, 3545-3547. (b) Ramakrishna, V.; Duke, B. J. *Inorg. Chem.* **2004**, *43*, 8176. (c) Sayin, H.; McKee, M. L. *Inorg. Chem.* **2007**, *46*, 2883. (d) Bühl, M.; McKee, M. L. *Inorg. Chem.* **1998**, *37*, 4953.

Chapter 3

Evaluating the Role of Triborane(7) as Catalyst in the Pyrolysis of Tetraborane(10)

3.1 Introduction

Pyrolyses of various boron hydrides have drawn much experimental attention.[1-9] The complexity of the reactions makes unraveling aspects of their kinetics daunting. In a previous study of the initial stage of diborane pyrolysis, we showed that even the simplest boron hydride, B_2H_6, presented considerable challenges.[10] As the second smallest stable boron hydride, B_4H_{10} [tetraborane(10)] also plays an important role in thermal reactions of boron hydrides thermal reactions.[11] There is still doubt concerning the mechanism and even the initial order of the reaction.[12-15]

Two reactions (1a) and (1b), both first order in B_4H_{10}, have been claimed to be the rate-limiting step in the initial stages of pyrolysis.[16-23] Reaction 1a was

$$B_4H_{10} \rightarrow B_4H_8 + H_2 \qquad (1a)$$

$$B_4H_{10} \rightarrow B_3H_7 + BH_3 \qquad (1b)$$

proposed as the rate-determining step from several experimental observations. First, the reaction between B_4H_{10} and ethylene yielded $B_4H_8(C_2H_4)$ while the reaction between deuterated ethylene and B_4H_{10} yielded $B_4H_8(C_2D_4)$.[24-25] Next, $B_4H_8D_2$ was captured as the product of the reaction between B_4H_8CO and D_2.[16] Also, mass-spectrometric analysis supported B_4H_8 but not BH_3 or B_3H_7 as a reactive intermediate.[19,20,22] Later publications

by Greenwood and co-workers[4,5] were consistent with the proposal of reaction 1a as the rate-limiting step. However, Koski[23] excluded reaction 1a based on their observation that D_2 did not exchange with B_4H_{10}, leading Greatrex *et al.*[4a,6] to suggest that the observation was a "worrying inconsistency in urgent need of reinvestigation". Nevertheless, Long[14] partially followed the mechanism of B_4H_{10} pyrolysis suggested by Koski.

It is well established that the initial stage of B_4H_{10} pyrolysis is first order in the B_4H_{10} concentration in the temperature range 293 to 333 K,[4,5] with an observed activation energy of 23.7 kcal/mol. It is worth noting that Koski reported a 3/2 order dependence on the B_4H_{10} concentration with a very low activation energy of 16.2 kcal/mol (Table 1).[23] Greenwood and co-workers[6] found that added hydrogen inhibited B_4H_{10} pyrolysis while the reaction order and activation energy remained unchanged. The elimination of H_2 and BH_3 from B_4H_{10} was studied computationally by McKee.[26a] At the estimated MP4/6-311G(d,p)//MP2/6-31G(d) level of theory with corrections to 400 K, the enthalpy of activation for loss of H_2 was 26.8 kcal/mol and for loss of BH_3 was estimated to be 39.0 kcal/mol. The former value was fortuitously close to the experimental value of 23.7 kcal/mol reported by Greenwood and co-workers for pyrolysis of B_4H_{10}.[4,5]

Several theoretical studies have focused on different isomers of B_4H_{10} and B_4H_8.[26,27] For example, Ramakrishna and Duke[27b] considered six isomers of B_4H_{10} and computed their interconversion pathways. Relative energies for various boron hydrides and several borane pyrolytic reactions associated with B_4H_{10} were also calculated.[28] In this work, the pyrolysis mechanism of B_4H_{10} has been explored at the G4 level of theory.

Table 1.Reaction activation energy (kcal/mol) of pyrolysis of B_4H_{10}

ΔE_a	Order	Temperature (K)	Year	Ref
Experiment				
16.2	1.5	313-333	1969	23
23.71±0.19	1.0	313-351	1984	4a
23.76±0.81	1.0	313-351	1986	4b
23.52±0.33[a]	1.0	313-351	1989	5
Calculation				
26.8	1.0	400	1990	27
35.0(eq 1a)	1.0	333	2013	this work
21.2(eq 3)	1.0[b]	333	2013	this work

a) The activation energy was measured in the presence of added H_2.

b) The ratio of $[B_3H_7]/[H_2]$ was assumed to be constant at 1.2×10^{-4}.

3.2 Computational methods

All the standard calculations were carried out with the Gaussian 09 package.[29] All boron hydrides were optimized and harmonic frequencies were calculated using B3LYP/6-31G(2df,p) which is part of the G4 composite method.[30] The connection between the reactant and product through a specific transition structure was obtained through the intrinsic reaction coordinate (IRC) method.[31]

The minimum energy path (MEP) for the barrierless dissociation of B_4H_{10}(b) to B_3H_7 and BH_3 was constructed by constrained optimization. The B-B distance was varied from 3.1 to 1.9 Å with a step size of 0.1 Å and all other variables were optimized via B3LYP/6-31G(2df,p). Single-point energy calculations along the reaction path were made at the G4 level of theory. The transition vector was projected out of the Hessian for points along the reaction path.

The zero-point corrections, heat capacity corrections, and entropies were computed to evaluate equilibrium constants using $K_p=\exp(-\Delta G^o/RT)$. Dual-level direct

dynamics method (VTST[32,33]-ISPE[34]) was employed to calculate the rate constant of $B_4H_{10} \rightarrow B_4H_8 + H_2$ where the lower level of theory was B3LYP/6-31G(2df,p) and the higher level of theory (used for reactant, transition structure, and products) was G4 theory.

3.3 Results and Discussion

3.3.A. Unimolecular B_4H_{10} Reactions

The elimination of H_2 from B_4H_{10} was thoroughly studied at the G4 level (Figure 1) where good agreement was found with a previous study[26] of the same reaction ($B_4H_{10}(a) \rightarrow TS(ad) \rightarrow B_4H_8 + H_2$) at the approximate MP2/6-31G(d) level. The transition structure is very late as judged by the short H-H distance in TS(ad) (0.7574 Å). The activation barrier for loss of H_2 using G4 theory at 0 K (33.8 kcal/mol) is 7.0 higher than the value reported previously (400 K) and 10 kcal/mol larger than the experiment value reported by Greenwood and co-workers[4,5] at 333 K. The large difference between theory and experiment may indicate that eq 1a is not the rate-determining step in B_4H_{10} pyrolysis as has been previously assumed.

To further verify the accuracy of the G4 level, other levels of theory were used to determine the activation barrier including the highest level used in this study, W1BD. As can be seen in Table 2, the G4 and W1BD levels agree to within 1 kcal/mol.

In B_4H_{10}, loss of BH_3 is preceded by the isomerization to a higher-energy isomer $B_4H_{10}(b)$ which is less stable than $B_4H_{10}(a)$ by 10.5 kcal/mol and separated by a 27.9 kcal/mol transition structure (TS(ab)). The values from a previous study at the estimated MP4/6-311+G(d,p)+ZPC level were 10.4 and 26.9 kcal/mol, respectively.[26a] Duke *et*

al.[26b] calculated 13.0 and 22.5 kcal/mol at the MP2/6-31G(d,p), respectively. The loss of BH_3 from B_4H_{10}(b) is endothermic by 28.2 kcal/mol at 0 K with no reverse activation barrier.

Table 2 Comparison of calculated energy barriers (kcal/mol) at 333 K

Level of theory	$B_4H_{10} \rightarrow B_4H_8+H_2$		$B_4H_{10} \rightarrow B_3H_7+BH_3$[b]			
	TST/VTST		TST		VTST	
	$\Delta H^{\ddagger}$	$\Delta G^{\ddagger}$	$\Delta H^{\ddagger}$	$\Delta G^{\ddagger}$	$\Delta H^{\ddagger}$	$\Delta G^{\ddagger}$
W1BD	34.3	33.0	41.3	28.0	39.0	35.1
G4	34.3	33.1	40.7	27.5	38.2	34.1
MP2/aug-cc-pVTZ	35.7	34.2	45.0	26.7		
B3LYP/6-31G(2df,p)	32.3	31.0			29.8	29.7
MP4/6-311G(d,p)[a]	26.8		39			
VTST-ISPE[c]	32.4	31.4				

a) Estimated at 400 K, also see Ref 26a.

b) The reaction path at G4 level of theory is shown in Figure 5. For W1BD reaction path, the G4 geometry at each point was re-optimized at the W1BD level of theory. Vibrational frequencies along the reaction path were calculated after projecting out the reaction coordinate.

c) Dual-level direct dynamics (VTST-ISPE) is used where B3LYP/6-31G(2df,p) is the low-level and G4 is the high-level. The $\Delta H^{\ddagger}$ and $\Delta G^{\ddagger}$ values were obtained from the activation energy and rate constant at 333 K from the VTST-ISPE results.

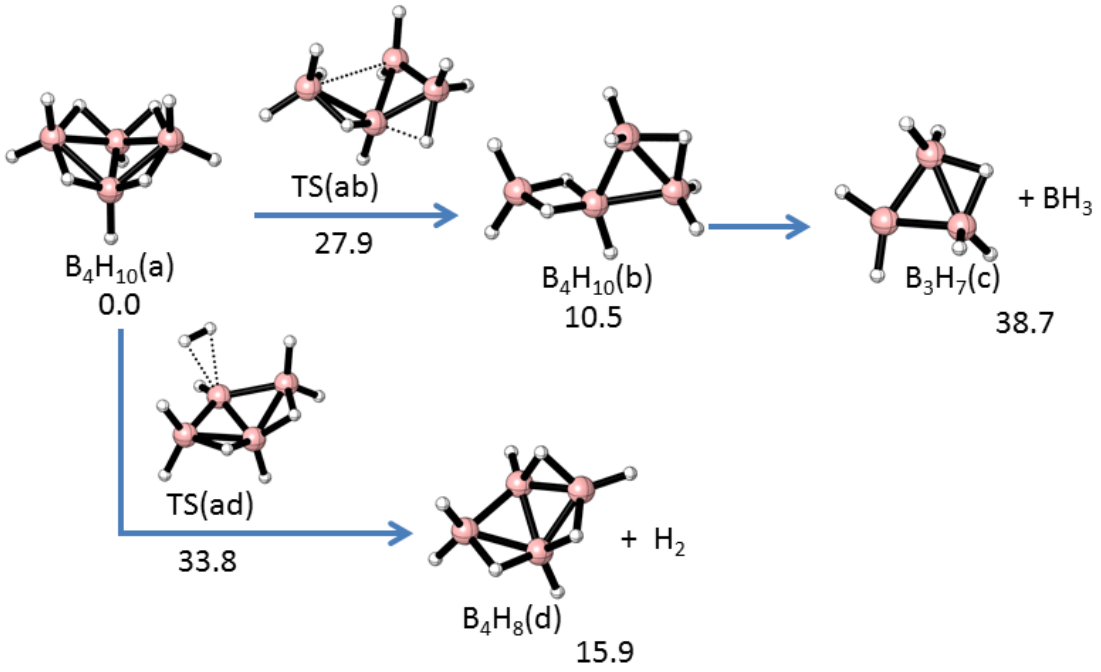

Figure 1. Enthalpy (kcal/mol) path at 0 K for the reaction of $B_4H_{10} \rightarrow B_3H_7 + BH_3$ and $B_4H_{10} \rightarrow B_4H_8 + H_2$. Enthalpy of B_4H_{10}(a) is taken as zero.

B_4H_{10} + BH_3: The schematic enthalpy (0 K) diagram of the B_4H_{10} + BH_3 reaction (Figure 2) is initiated with the barrierless association to form a B_4H_{10}-BH_3 complex (B_5H_{13}(e)). The complex can then either surmount an 8.0 kcal/mol barrier to form B_3H_7(c) plus diborane through transition structure TS(ef) ($\Delta H^{\ddagger}$=8.0 kcal/mol) or eliminate H_2 to form B_5H_{11}(g) through transition structure TS(eg) ($\Delta H^{\ddagger}$=12.7 (9.7+3.0) kcal/mol). Structure B_5H_{11}(g) is a newly reported isomer of B_5H_{11} with a BH_2 group replacing a terminal hydrogen of B_4H_{10}. The barrier from B_5H_{11}(g) to

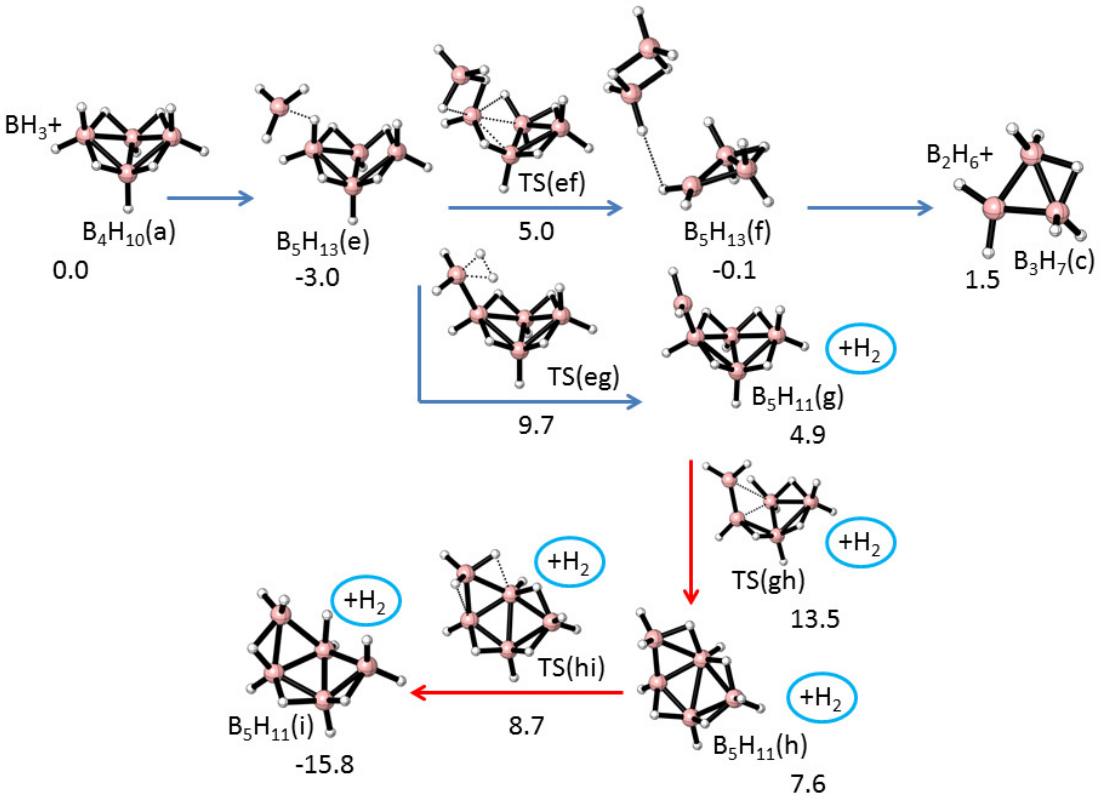

Figure 2. Enthalpy (kcal/mol) path at 0 K for the reaction of $B_4H_{10}(a) + BH_3 \rightarrow B_3H_7(c) + B_2H_6$ and $B_4H_{10}(a) + BH_3 \rightarrow B_5H_{11}(i) + H_2$. Enthalpies of $B_4H_{10}(a) + BH_3$ are taken as zero. The hydrogen in circle represents that the formed hydrogen does not involve in the following reactions.

B_5H_{11} (h) and finally to the experimentally observed $B_5H_{11}(i)$ is low due to the empty orbital on the terminal BH_2 group. The path to $B_2H_6 + B_3H_7(c)$ should dominate over the path to $B_5H_{11}(g)$ since the barrier is 4.7 kcal/mol smaller at 0 K which rules out BH_3 as a catalyst in the reaction $B_4H_{10} + BH_3 \rightarrow H_2 + B_5H_{11} \rightarrow B_4H_8 + BH_3$.

B_4H_{10} + B_3H_7: $B_4H_{10}(a) + B_3H_7(c)$ will barrierlessly associate to B_4H_{10}-B_3H_7 ($B_7H_{17}(j)$)

which can further form B_7H_{17}(k) through transition structure TS(jk) ($\Delta H^{\ddagger}$=8.9 kcal/mol, Figure 3). B_7H_{17}(k) can be viewed as a coupled-cage of B_3H_9 and B_4H_{10}(a) with a B-B single bond which can release B_2H_6 through a 19.8 kcal/mol barrier via TS(kg) or release H_2 to form B_7H_{15}(l) via transition structure TS(kl) with an activation barrier of 9.6 kcal/mol. B_7H_{15}(l) can rearrange through three intermediates, B_7H_{15}(m), B_7H_{15}(n), B_7H_{15}(o) to form B_4H_8(d) plus B_3H_7(c). The overall reaction is B_4H_{10}(a) + B_3H_7(c) → B_4H_8(d) + H_2 + B_3H_7(c) which shows that B_3H_7 can catalyze the elimination of H_2 from B_4H_{10}.

B_4H_{10} + B_4H_8: The PES diagram with zero-point energy corrections of B_4H_{10}(a) + B_4H_8(d) is shown in Figure 4. The first intermediate formed is a C_2-symmetry B_8H_{18}(p) species which is a coupled-cage of two B_4H_{10} boron hydrides (with two terminal hydrogen atoms removed). The transition structure TS(pq) which connects B_8H_{18}(p) and B_8H_{18}(q) is analogous to the B_4H_{10}(a) → TS(ab) → B_4H_{10}(b) step in Figure 1 with corresponding activation barriers of 26.9 and 27.9 kcal/mol, respectively; intermediate B_8H_{18}(q) has a pentacoordinated boron center. B_8H_{18}(q) can form B_5H_{11}(g) + B_3H_7(d) without a reverse activation barrier. The conversion of B_5H_{11}(g) to B_5H_{11}(i) was discussed above.

B_8H_{18}(p) can also release hydrogen to form B_8H_{16}(r) through transition structure TS(pr) which is analogous to B_4H_{10}(a) → TS(ad) → B_4H_8(d) + H_2 in Figure 1 with corresponding activation barriers of 32.8 and 33.8 kcal/mol, respectively. From B_8H_{16}(r), the reaction proceeds through B_8H_{16}(s) and then to two B_4H_8(d). The overall reactions

form either B_3H_7(c) plus B_5H_{11}(i) or two B_4H_8(d) plus H_2. As noted below, the two paths have very similar activation

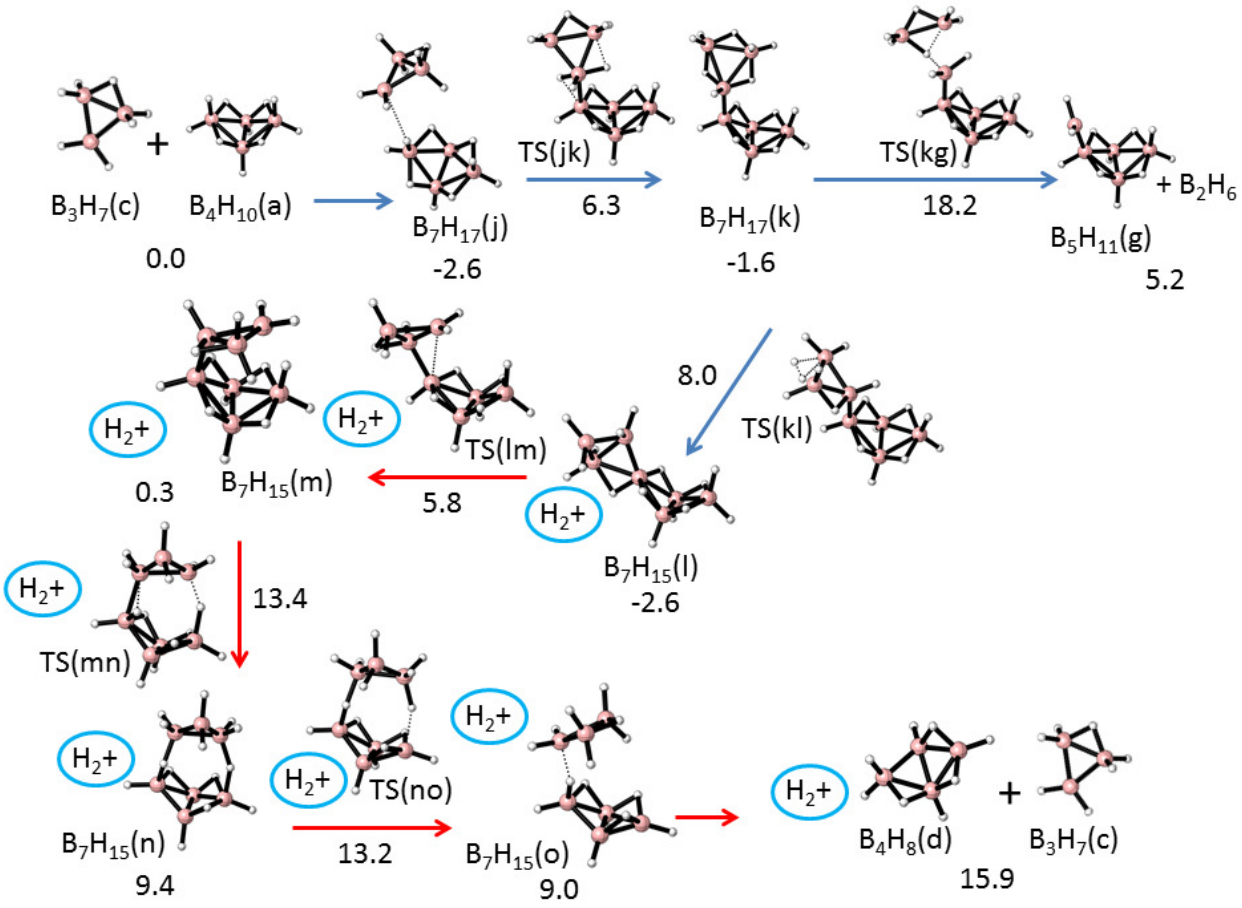

Figure 3. Enthalpy (kcal/mol) path at 0 K for the reaction of B_4H_{10}(a) + B_3H_7(c) → B_5H_{11}(g) + B_2H_6 and B_4H_{10}(a) + B_3H_7(c) → B_4H_8(d) + H_2 + B_3H_7(c). Enthalpies of B_4H_{10}(a) + B_3H_7(c) are taken as zero. The hydrogen in circle represents that the formed hydrogen does not involve in the following reactions.

barriers with a slight edge in free energy to the reaction forming B_3H_7(c)/B_5H_{11}(i).

3.3.B. TST versus VTST

It has been assumed that the pyrolysis of B_4H_{10} is initialized by the elimination of hydrogen since the reaction is known to be first order in B_4H_{10} concentration. A counterexample is from a study by Bond and Pinsky who found that the reaction was 3/2 order in B_4H_{10}.[15] However, the reliability of their experiment observations has been questioned by Greenwood.[4] The free energy paths of $B_4H_{10}(a) \rightarrow B_4H_8(d) + H_2$ and $B_4H_{10}(a) \rightarrow B_4H_{10}(b)$ are straightforward since they both have tight transition structures. However the dissociation of $B_4H_{10}(b)$ to $B_3H_7(c) + BH_3$ is a barrierless reaction, which requires application of variational transition state theory (VTST). In this method, a series of structures along the reaction path were calculated and the free energies determined at each point. The maximum free energy along the path at temperature T determines the transition state, *i.e.* the bottleneck. In the $B_4H_{10} \rightarrow BH_3 + B_3H_7$ reaction, the reaction path was constructed where the B-B distance was decreased in 0.1 Å steps from 3.1 to 1.9 Å, a range where all of the vibrational modes were positive after projecting out the transition vector (Figure 5). The free energy maximum is 6.6 kcal/mol higher than separated BH_3 and $B_3H_7(c)$ (Figure 6). This result is also consistent with our previous study of the dissociation path of diborane, another barrierless reaction. At the G4 level, the free energy maximum on the dissociation path of diborane was 6.7 kcal/mol at 420 K larger than two separated BH_3 units.[10]

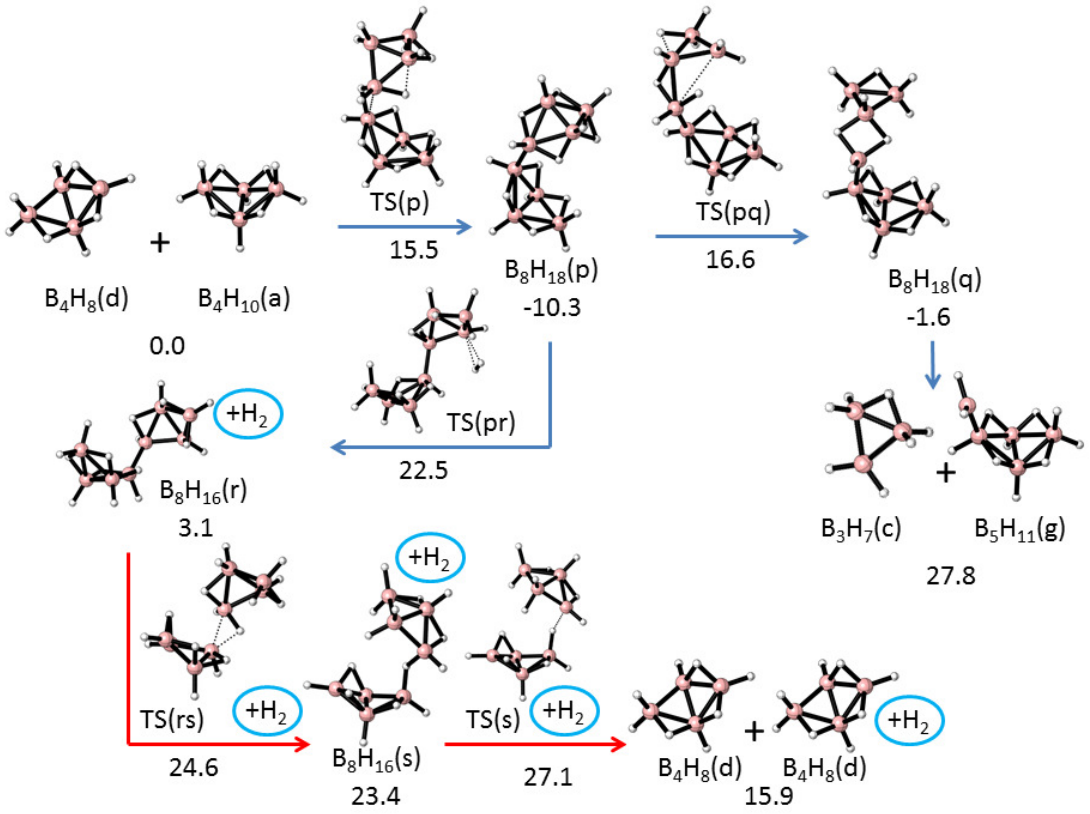

Figure 4. Enthalpy (kcal/mol) path at 0 K for the reaction of $B_4H_{10}(a) + B_4H_8(d) \rightarrow B_5H_{11}(g) + B_3H_7(c)$ and $B_4H_{10}(a) + B_4H_8(d) \rightarrow B_4H_8(d) + H_2 + B4H_8(c)$. Enthalpies of $B_4H_{10}(a) + B_3H_7(c)$ are taken as zero. The hydrogen in circle represents that the formed hydrogen does not involve in the following reactions.

When 6.6 kcal/mol is added to the free energy of $B_3H_7(c) + BH_3$, the activation free energy $B_4H_{10}(a) \rightarrow B_4H_8(d) + H_2$ is more favorable by 1.0 kcal/mol than $B_4H_{10}(a) \rightarrow B_3H_7(c) + BH_3$ at 333 K. The preference does not change at different temperatures as seen in Table 3.

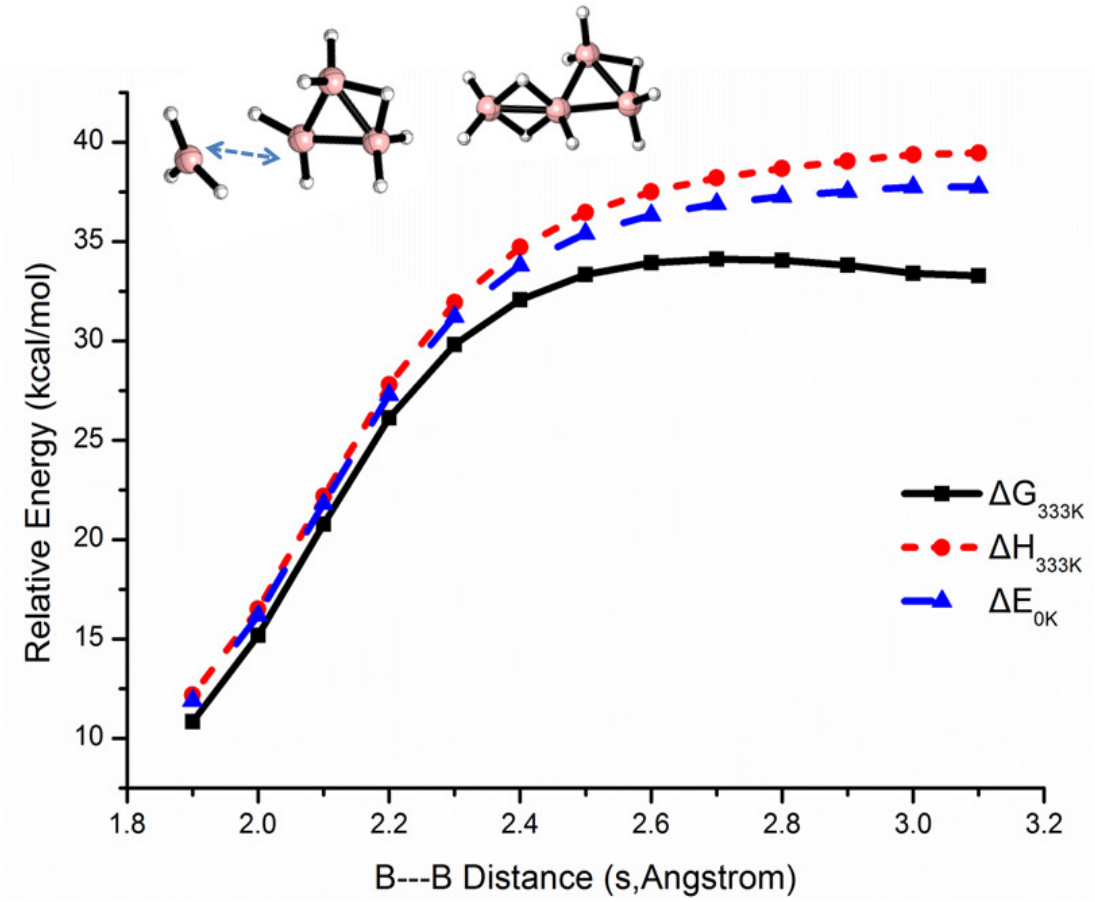

Figure 5. Reaction paths for dissociation of B4H10(b) → BH3 + B3H7(c). Quantities calculated at G4 level of theory are enthalpies (333 K), free energies (333 K), and entropies (0 K). The quantities of B4H10(b) at infinity distance have been taken as zero. The distance of enlarging B-B bond in B4H10(b) has been taken as the calibration for the reaction paths (The arrow connects the two boron atoms). The reaction coordinate has been projected out.

From our above discussion, BH_3, B_3H_7(c) and B_4H_8(d) can all serve as scavenging species to accelerate the consumption of B_4H_{10} (Table 4). The free

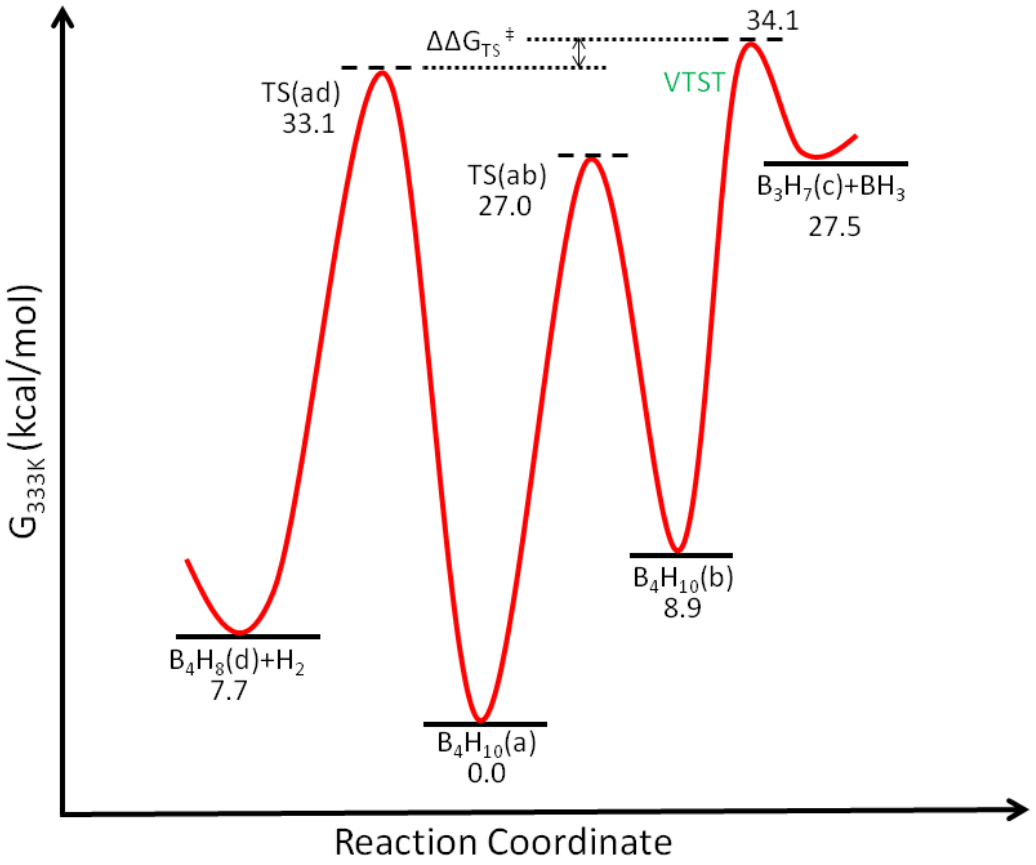

Figure 6. Comparison of free energy (kcal/mol) path at 333 K for the reaction of B_4H_{10}(a) → B_4H_8(d) + H_2 and B_4H_{10}(a) → B_3H_7(c) + BH_3. Free energy of B_4H_{10}(a) is taken as zero.

energy barriers for the reaction of B_4H_{10} + BH_3 and B_4H_{10} + B_3H_7 are significantly smaller than that of B_4H_{10} + B_4H_8 ($\Delta G^{\ddagger}$=14.8 and 19.7 compared to 33.2 kcal/mol at 333 K). Of the two unimolecular reactions of B_4H_{10}, the elimination of H_2 is slightly favored over the elimination of BH_3. Another piece of evidence suggesting that generation of BH_3 is not important as the initial step is the fact that B_2H_6 is not formed in early stages of B_4H_{10} pyrolysis which would be expected from the dimerization of BH_3. Also, the

formation of BH_3 should slow the consumption of B_4H_{10} because B_2H_6 (formed from $2BH_3$ without activation barrier) can react further with B_3H_7(c) to form BH_3 plus B_4H_{10}. Greenwood *et al*.[4] also suggested elimination of H_2 as the initial step from a similar analysis of the experimental data.

Table 3. Comparison of calculated free energy barriers (kcal/mol) at different temperatures at the G4 level of theory

	373K	333K	313K	293K
$B_4H_{10}\rightarrow B_4H_8+H_2$	32.95	33.10	33.17	33.24
$B_4H_{10}\rightarrow B_3H_7+BH_3$	34.02	34.12	34.36	35.02

Table 4. Calculated reaction activation enthalpies, reaction activation free energies, reaction heats and reaction free energies (kcal/mol) at 333 K with G4 level of theory[a]

	$\Delta H^{\neq}$	$\Delta G^{\neq}$	ΔH	ΔG
$B_4H_{10}\rightarrow B_3H_7+BH_3$[b]	38.2	34.1	40.7	27.5
$B_4H_{10}\rightarrow B_4H_8+H_2$	34.3	33.1	17.7	7.7
$B_4H_{10}+BH_3\rightarrow B_2H_6+B_3H_7$	4.0	14.8	1.4	-0.2
$B_4H_{10}+BH_3\rightarrow B_5H_{11}+H_2$	8.5	19.9	-15.6	-12.9
$B_4H_{10}+B_3H_7\rightarrow B_4H_8+H_2+B_3H_7$	17.7	19.2	17.7	7.7
$B_4H_{10}+B_4H_8\rightarrow B_3H_7+B_5H_{11}$[b]	28.8	33.2	28.8	26.6
$B_4H_{10}+B_4H_8\rightarrow B_4H_8+B_4H_8+H_2$	22.7	34.7	17.7	7.7

a) Values for the overall reaction. For example, $B_4H_{10}\rightarrow BH_3+B_3H_7$ represents B_4H_{10}(a) forming the final products BH_3 and B_3H_7(c).

b) The free energy maximum of $B_4H_{10}\rightarrow BH_3+B_3H_7$ is 6.6 kcal/mol higher than the separated BH_3 and B_3H_7. Thus, 6.6 kcal/mol was added to the ΔG of B_3H_7 + B_5H_{11} to estimate the free energy maximum of $B_4H_{10}+B_4H_8\rightarrow B_3H_7+B_5H_{11}$. Also see details in text.

3.3.C. Role of B_3H_7 and B_4H_8 as catalyst

To explore B_3H_7 as a catalyst in more detail, enthalpies (0 K and 333 K) and free energies (333 K) are given in Figure 7 for reactants, intermediates, transition structures, and products in the $B_4H_{10}(a) + B_3H_7(c) \rightarrow B_4H_8(d) + H_2 + B_3H_7(c)$ reaction as well as for the direct reaction $B_4H_{10}(a) \rightarrow B_4H_8(d) + H_2$. The activation barrier decreases significantly for the catalyzed reaction compared to the uncatalyzed one ($\Delta H^{\ddagger}$=17.7 to 34.3 kcal/mol at 333 K). The reaction path for the catalyzed reaction has six intermediates and can be divided into three stages (Figure 7): formation of B_7H_{17}, elimination of H_2, and decomposition of B_7H_{15} into $B_3H_7 + B_4H_8$. A coupled-cage is formed between B_3H_7 and B_4H_{10} in the first step to ($B_7H_{17}(k)$). In the second stage, H_2 is lost from the B_3H_7 portion of the coupled-cage. The activation barrier for loss of H_2 ($B_7H_{17}(kl)$) is very similar to the barrier for loss of H_2 from B_3H_9-C_{3v} ($\Delta H^{\ddagger}$=10.2 to 11.7 kcal/mol at 333 K). In the third stage, the coupled-cage $B_7H_{15}(m)$ undergoes a hydrogen atom transfer to generate $B_7H_{15}(o)$ which decomposes to $B_3H_7(c)$ plus $B_4H_8(d)$.

The B_4H_8 intermediate can also act as a catalyst as shown in Figure 8 by the reactions $B_4H_{10}(a) + B_4H_8(d) \rightarrow B_4H_8(d) + B_4H_8(d) + H_2$ and $B_4H_{10}(a) \rightarrow B_4H_8(d) + H_2$ (enthalpies at 0 K and 333 K and free energies at 333 K). Similar to B_3H_7, B_4H_8 lowers the activation barrier for loss of H_2 from B_4H_{10} relative to the uncatalyzed reaction ($\Delta H^{\ddagger}$=22.7 vs 34.3 kcal/mol at 333 K). However, the effect of entropy cancels the advantage and the catalyzed reaction actually has a larger free energy of

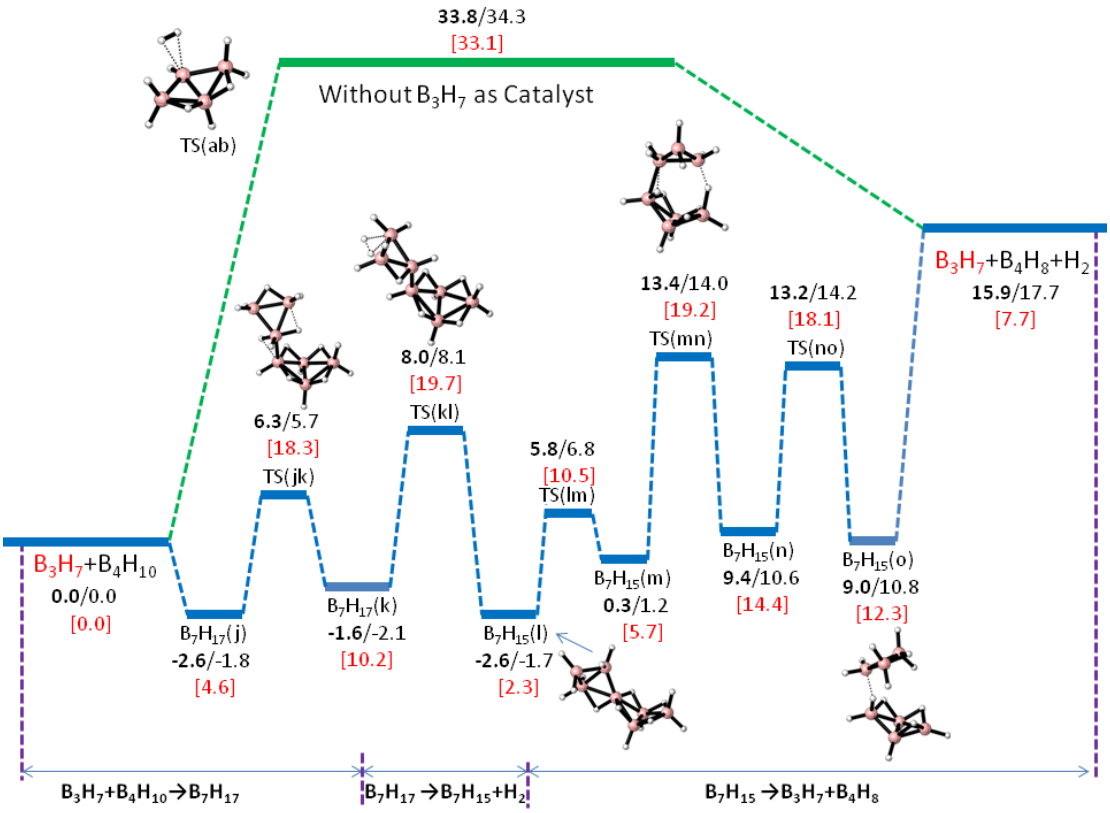

Figure 7. Comparison of activation enthalpy (kcal/mol) path at 0 K for the reaction of $B_4H_{10}(a) \rightarrow B_4H_8(d) + H_2$ and $B_4H_{10}(a) + B_3H_7(c) \rightarrow B_3H_7(c) + B_4H_8(d) + H_2$. Enthalpies and free energy of $B_4H_{10}(a)$ are taken as zero. Enthalpies and free energy of $B_4H_{10}(a) + B_3H_7(c)$ are taken as zero. All the numbers on the path are calibrated to the relative zero point and their format is as following: Enthalpy (0 K)/Enthalpy (333 k) and the number in the square bracket is free energy at 333 K. The entire reaction can be divided into three stages: formation of B_7H_{17}, elimination of H_2, and decomposition of B_7H_{15} into $B_3H_7 + B_4H_8$. All the geometries of transition structures and stationary points in the curves can be found in Figure 3.

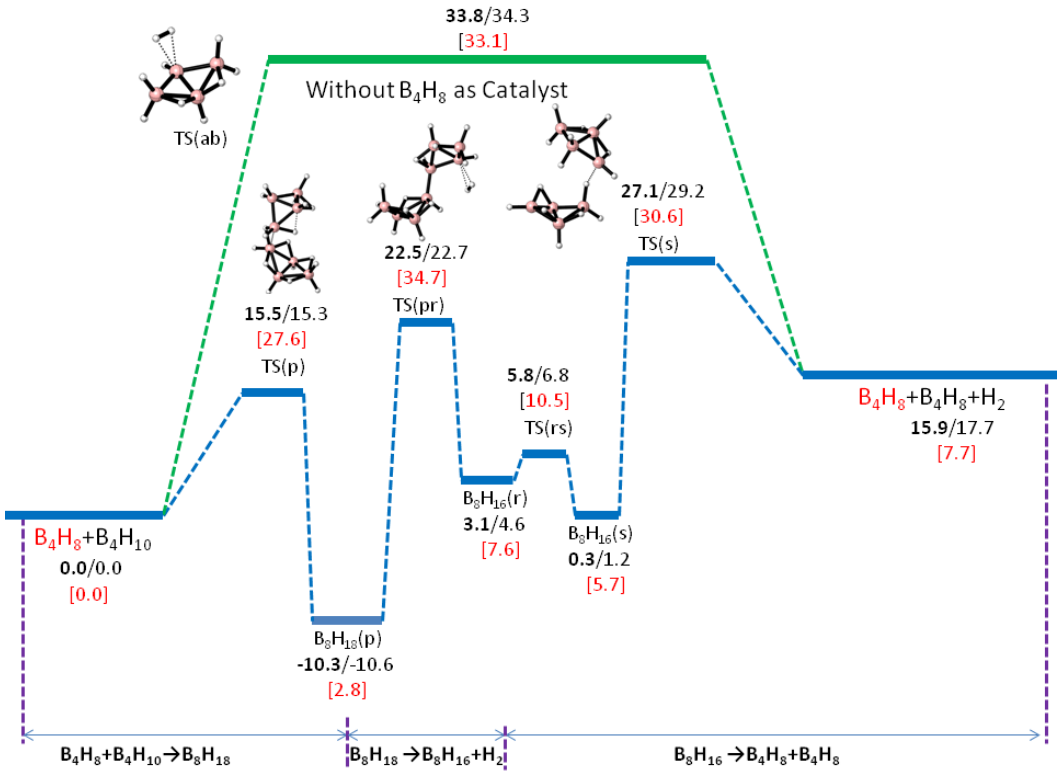

Figure 8. Comparison of activation enthalpy (kcal/mol) path at 0 K Enthalpies and free energy of B_4H_{10}(a) are taken as zero. Enthalpies and free energy of B_4H_{10}(a) + B_4H_8(d) are taken as zero. All the numbers on the path are calibrated to the relative zero point and their format is as following: Enthalpy (0 K)/Enthalpy (333 k) and the number in the square bracket is free energy at 333 K. The entire reaction can be divided into three stages: formation of B_8H_{18}, elimination of H_2, and decomposition of B_8H_{16} into B_4H_8 + B_4H_8. In the range of $B_8H_{16} \rightarrow B_4H_8$(d) + B_4H_8(d), the energy properties of H_2 are also added to the path. All the geometries of transition structures and stationary points in the curves can be found in Figure 4.

activation at 333 K compared to the uncatalyzed reaction ($\Delta G^{\ddagger}$=34.7 to 33.1 kcal/mol at 333 K). The mechanism is similar to the B_3H_7 + B_4H_{10} reaction. A C_2-symmetry

coupled-cage between two B_4H_9 fragments is formed (B_8H_{18}(p)) which loses H_2 from one side. The resulting coupled-cage between B_4H_7 and B_4H_9 (B_8H_{16}(r)) migrates a hydrogen atom (from the B_4H_9 side to the B_4H_7 side) and fragments to two B_4H_8(d) species.

3.3.D. Pyrolysis Mechanism

Several mechanisms of the initial stage of B_4H_{10} pyrolysis have been proposed.[3,4] One typical example[4] is eq 1a,c:

$$B_4H_{10} \rightarrow B_4H_8 + H_2 \quad (1a)$$

$$B_4H_{10} + B_4H_8 \rightarrow B_3H_7 + B_5H_{11} \quad (1c)$$

where eq 1a is the rate-limiting step. The reactions that may be involved in the pyrolysis are presented as following:

$$B_4H_{10} \rightarrow B_4H_8 + H_2 \quad (1a)$$

$$B_4H_{10}(a) \rightleftarrows B_4H_{10}(b) \quad (2b)$$

$$B_4H_{10}(b) \rightarrow B_3H_7 + BH_3 \quad (2c)$$

$$B_4H_{10} + BH_3 \rightarrow B_2H_6 + B_3H_7 \quad (2d)$$

$$B_4H_{10} + B_3H_7 \rightleftarrows B_7H_{17} \quad (2e)$$

$$B_7H_{17} \rightleftarrows B_7H_{15} + H_2 \quad (2f)$$

$$B_7H_{15} \rightarrow B_3H_7 + B_4H_8 \quad (2g)$$

$$B_4H_{10} + B_4H_8 \rightarrow B_3H_7 + B_5H_{11} \quad (1c)$$

$$B_4H_{10} + B_4H_8 \rightarrow B_4H_8 + B_4H_8 + H_2 \quad (2h)$$

$$B_3H_7 + B_3H_7 \rightarrow \text{Solid} + mH_2 \quad (2i)$$

From our previous discussion, eq 2b-2d are not important.

The reaction mechanism can be summarized in Figure 9. Briefly, B_4H_{10} eliminates hydrogen, then B_4H_8 reacts with B_4H_{10} to produce B_5H_{11} and B_3H_7. B_3H_7 can then catalyze elimination of H_2 from B_4H_{10} which forms more B_4H_8 and generates more B_3H_7 which will accumulate and polymerize to a solid.

We propose the following mechanism:

Initiation:	$B_4H_{10} \rightarrow B_4H_8 + H_2$	k_0	(1a)
Propagation:	$B_4H_{10} + B_3H_7 \rightleftarrows B_7H_{17}$	k_1, k_{-1}, K_1	(2e)
	$B_7H_{17} \rightleftarrows B_7H_{15} + H_2$	k_2, k_{-2}, K_2	(2f)
	$B_7H_{15} \rightarrow B_4H_8 + B_3H_7$	k_3	(2g)
	$B_4H_{10} + B_4H_8 \rightarrow B_3H_7 + B_5H_{11}$	k_4	(1c)
Termination:	$B_3H_7 + B_3H_7 \rightarrow$ Solid + mH_2		(2i)

where the overall reaction is $2B_4H_{10} \rightarrow B_5H_{11} + H_2 + B_3H_7$ in propagation stage and $2B_4H_{10} \rightarrow B_5H_{11} + (1+m)H_2$ in propagation plus termination stages.

It is worthwhile to discuss how the experimental data were collected. The species (B_4H_{10}, B_5H_{11}, H_2) in the gas mixture were collected after a particular time interval of at least 60s after the reaction started. Even at the very first experimental point, both H_2 and B_5H_{11} were already produced. Thus, the experimental rate measurements may take place after the incubation period where the catalytic boron hydride B_3H_7 is formed. In our mechanism, the experimentally collected data should be associated with the second stage (Propagation) in the Figure 9. The

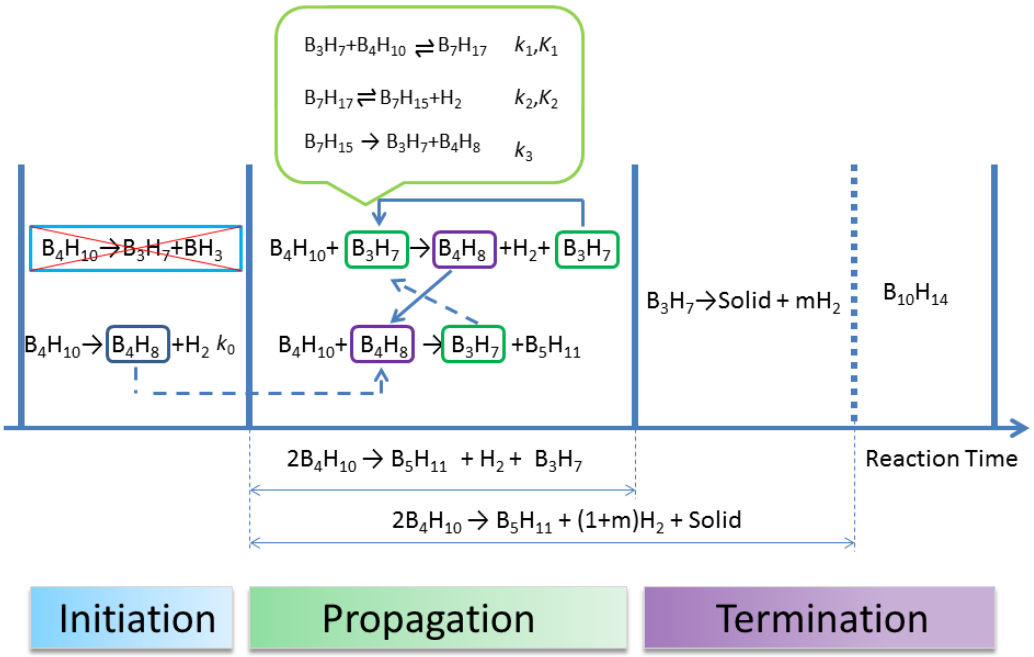

Figure 9. Schematic mechanism diagram of B_4H_{10} pyrolysis. The reaction above the arrow represents the overall reaction during the arrow pointed range.

steady-state approximation is used to deduce the rate law (see section 3.4.A).

$$\frac{d(B_4H_{10})}{dt} = -2k_3K_1K_2[B_4H_{10}][B_3H_7]/[H_2] \qquad (3)$$

The mechanism in which reaction (1a) serves as the rate limiting step is inappropriate because the calculated activation barrier is about 10 kcal/mol higher than the experimental value (Table 1). For our mechanism to be consistent with the observed first order dependence on B_4H_{10} concentration, the ratio of $[B_3H_7]/[H_2]$ should be approximately constant. This ratio also can be estimated comparing the calculated rate constants to the experimentally observed ones. The experiment and calculated rates

agree if the ratio is 1.2 x 10^{-4} at 333 K (also see 3.4 B and 3.4..C) which is reasonable since B_3H_7 is a reactive intermediate. From the rate law in eq 3, the theoretically calculated activation energy of the B_4H_{10} pyrolysis is 21.2 kcal/mol (3.4 S-4). One issue with our mechanism is that one hydrogen is produced for each B_5H_{11} while the experimental ratio is approximately two. It is likely that the surplus hydrogen comes from the polymerization of B_3H_7 and B_4H_8 to a solid as well as from the reaction of $B_4H_{10}(a) + B_4H_8(d) \rightarrow B_4H_8(d) + B_4H_8(d) + H_2$. As the reaction proceeds, the reactive intermediates BH_3, B_3H_7 and B_4H_8 will react to form higher boron hydrides up to $B_{10}H_{14}$ (and release additional H_2).

3.4 Rate law deviation

3.4.A

$B_4H_{10} + B_3H_7 \rightleftarrows B_7H_{17}$ k_1, k_{-1}, K_1 (2e)

$B_7H_{17} \rightleftarrows B_7H_{15} + H_2$ k_2, k_{-2}, K_2 (2f)

$B_7H_{15} \rightarrow B_4H_8 + B_3H_7$ k_3 (2g)

$B_4H_{10} + B_4H_8 \rightarrow B_3H_7 + B_5H_{11}$ k_4 (1c)

$$\frac{d(B_4H_{10})}{dt} = -k_1[B_4H_{10}][B_3H_7]+k_{-1}[B_7H_{17}]-k_4[B_4H_{10}][B_4H_8] \quad \text{(SA-1)}$$

$$\frac{d(B_4H_8)}{dt} = k_3[B_7H_{15}]-k_4[B_4H_{10}][B_4H_8] = 0 \quad \text{(SA-2)}$$

$$\frac{d(B_7H_{17})}{dt} = k_1[B_4H_{10}][B_3H_7]-k_{-1}[B_7H_{17}]-k_2[B_7H_{17}]+k_{-2}[B_7H_{15}][H_2] = 0 \quad \text{(SA-3)}$$

$$\frac{d(B_7H_{15})}{dt} = k_2[B_7H_{17}]-k_{-2}[B_7H_{15}][H_2]-k_3[B_7H_{15}] = 0 \quad \text{(SA-4)}$$

Insert (SA-2), (SA-3), and (SA-4) into (SA-1):

$$\frac{d(B_4H_{10})}{dt} = -2k_3[B_7H_{15}] \quad \text{(SA-5)}$$

From (SA-1), (SA-2) and (SA-3),

$$[B_7H_{15}]=K_1k_2[B_4H_{10}][B_3H_7]/\{k_{-2}[H_2]+k_3+k_2k_3/k_{-1}\} \quad \text{(SA-6)}$$

$k_{-2}[H_2] >> k_3+k_2k_3/k_{-1}$

Therefore, $k_3[B_7H_{15}]=k_3K_1K_2[B_4H_{10}][B_3H_7]/[H_2]$ (SA-7)

$$\frac{d(B_4H_{10})}{dt} = -2k_3K_1K_2[B_4H_{10}][B_3H_7]/[H_2] \quad \text{(SA-8)}$$

We assume that the ratio $[B_3H_7]/[H_2] \approx$ constant

3.4.B. Plot for the pyrolysis of B_4H_{10}.

The experiment data from reference (4b) has been re-plotted according to the following equation:

$$k = K(k_BT/h)\cdot\exp(\Delta S^{\ddagger}/R)\cdot\exp(-\Delta H^{\ddagger}/RT) \quad \text{(SB-1)}$$

Thus, the experimentally observed activation free energy is 25.3 kcal/mol.

3.4.C. Estimated ratio of B_3H_7 to H_2. Transition state theory was applied (Equation S3-1).

$$k = (k_BT/h)\exp(-\Delta G^{\ddagger}/RT) \quad \text{(SC-1)}$$

$$k_{expt} = k = -2k_3K_1K_2[B_4H_{10}][B_3H_7]/[H_2] \quad \text{(SC-2)}$$

Therefore:

$$\exp(-\Delta G^{\ddagger}_{expt}/RT) = 2\exp(-\Delta G^{\ddagger}_3/RT)\cdot\exp(-\Delta G_1/RT)\cdot\exp(-\Delta G_2/RT)[B_3H_7]/[H_2] \quad \text{(SC-3)}$$

$\Delta G^{\ddagger}_{expt}$ is the experimentally observed activation free energy which is 25.3 kcal/mol. $\Delta G^{\ddagger}_3$, ΔG_1, and ΔG_2 are activation free energy of reaction (2g) and the reaction free energies of (2e) and (2f) the in S-1, respectively.

Insert $\Delta G^{\ddagger}_3 + \Delta G_1 + \Delta G_2$ at 333 K (19.2 kcal/mol) into equation (SC-3) to estimated the ratio of B_3H_7 to H_2 as 1.2×10^{-4}.

3.4.D. To calculate the activation energy the Arrhenius equation and the estimated ratio of B_3H_7 to H_2 are used.

$$k_{expt} = -2k_3K_1K_2[B_3H_7]/[H_2] \quad \text{(SD-1)}$$

According to the Arrhenius equation:

$$k = A \cdot \exp(-E_a/RT) \quad \text{(SD-2)}$$

$$A_{calc} \cdot \exp(-E_{calc}/RT)$$

$$= 2A_3 \cdot \exp(-(\Delta H^{\ddagger}_3 + RT))/RT) \cdot A_1 \cdot \exp(\Delta H_1/RT) \cdot A_2 \cdot \exp(\Delta H_2/RT)[B_3H_7]/[H_2] \quad \text{(SD-3)}$$

$$= 2A_3A_1A_2\exp(-(\Delta H^{\ddagger}_3 + RT + \Delta H_1 + \Delta H_2)[B_3H_7]/[H_2] \quad \text{(SD-4)}$$

Insert $\Delta H^{\ddagger}_3 + RT + \Delta H_1 + \Delta H_2$ at 333 K (14.6 kcal/mol),

$[B_3H_7]/[H_2] = \exp(-6.6(\text{kcal/mol})/RT)$

Thus, $E_{calc} = 14.6 + 6.6 = 21.2$ kcal/mol

$\Delta H^{\ddagger}_3$, ΔH_1, and ΔH_2 is the activation enthalpy of reaction (2g) and the reaction enthalpies of (2e) and (2f) in S-1, respectively.

3.5 Conclusion: The gas-phase kinetics of the initial stages of B_4H_{10} pyrolysis have been studied by accurate computational methods. Conventional transition state theory (TST) and variational transition state theory (VTST) have been employed to elucidate the reaction mechanism. The reaction $B_4H_{10} \rightarrow B_4H_8 + H_2$ can proceed with or without the

B_3H_7 catalysis with very different activation energies. The uncatalyzed reaction is considered as the initiation reaction. Thereafter, the hydrogen-releasing path will take place with B_3H_7 acting as a catalyst. As the reaction proceeds, hydrogen may be produced through the polymerization of intermediates. The overall activation energy is 21.2 kcal/mol which is about 2 kcal/mol smaller than the experimental values.

3.6 Reference:

(1) Stock, A. *The Hydrides of Boron and Silicon*, Cornell University Press: Ithaca, N.Y., 1933**,** p 250.

(2) Fehlner, T. P. In *Boron Hydride Chemistry*; Mutterties, E. L., Ed.; Academic Press: New York, 1975, p 175.

(3) Greatrex, R.; Greenwood, N. N.; Lucas, S. M. *J. Am. Chem. Soc*. **1989**, *111*, 8721.

(4) (a) Greatrex, R.; Greenwood, N. N.; Potter, C. D. *J. Chem. Soc*., Dalton Trans. **1984,** 2435. (b) Greatrex, R.; Greenwood, N. N.; Potter, C. D. *J. Chem. Soc., Dalton Trans.* **1986,** 81.

(5) Attwood, M. D.; Greatrex, R.; Greenwood, N. N. *J. Chem. Soc., Dalton Trans*. **1989,** 385.

(6) Attwood, M. D.; Greatrex, R.; Greenwood, N. N. *J. Chem. Soc., Dalton Trans.* **1989,** 391.

(7) Greatrex, R.; Greenwood, N. N.; Jump, G. A. *J. Chem. Soc., Dalton Trans.* **1985,** 541.

(8) Greatrex, R.; Greenwood, N. N.; Waterworth, S. D. *J. Chem. Soc., Chem. Commun.* **1988,** 925.

(9) Greenwood, N. N.; Greatrex, R. *Pure Appl. Chem.* **1987,** *59,* 857.

(10) Sun, B.; McKee, M. L. *Inorg. Chem.* **2013**, *52*, 5962.

(11) Greenwood, N. N. *Chem. Soc. Rev.* **1992,** *21*, 49.

(12) Dupont, J. A.; Schaeffer, R., *J. Inorg. Nucl. Chem.* **1960,** *15,* 310.

(13) Brennan, G. L.; Schaeffer, R., *J. Inorg. Nucl. Chem.* **1961,** *20,* 205.

(14) Long, L. H. *J. Inorg. Nucl. Chem.* **1970,** *32,* 1097.

(15) Bond, A. C.; Pinsky, H. L. *J. Am. Chem. Soc.* **1970,** *92,* 32.

(16) Norman, A. D.; Schaeffer, R. *J. Am. Chem. Soc.* **1966,** *88,* 1143.

(17) Norman, A. D.; Schaeffer, R.; Baylis, A. B.; Pressley, G. A.; Stafford, F. E. *J. Am. Chem. Soc.* **1966,** *88,* 2151.

(18) Schaeffer, R.; Sneddon, L. G. *Inorg. Chem.* **1972,** *11,* 3098.

(19) Baylis, A.; Pressley, G. A.; Gordon, M. E.; Stafford, F. E. *J. Am. Chem. Soc.* **1966**, *88,* 929.

(20) Hollins, R. E.; Stafford, F. E. *Inorg. Chem.* **1970,** *9,* 877.

(21) Stafford, F. E. *Bull. Soc. Chem. Belg.* **1972,** *81,* 81.

(22) Ganguli, P. S.; Gordon, L. P.; McGee, H. A. *J. Chem. Phys.* **1970,** *53,* 182.

(23) Koski, W. S. *Adv. Chem. Ser.* **1961,** *32,* 78.

(24) Harrison, B. C.; Solomon, I. J.; Hites, R. D.; Klein, M. J. *J. Inorg. Nucl. Chem.* **1960,** *14,* 195.

(25) Williams, R. E.; Gerhart, F. J. *J. Organomet. Chem.* **1967,** *10,* 168.

(26) (a) McKee, M. L. *J. Am. Chem. Soc.* **1990,** *112,* 19. (b) Ramakrishna, V.; Duke, J. B. *Inorg. Chem.* **2004,** *43,* 8176. (c) McKee, M. L. *Inorg. Chem.* **1986,** *25,* 3545.

(27) Tian, S. X. *J. Phys. Chem. A* **2005**, *109*, 5471.

(28) Bühl, M.; McKee, M. L. *Inorg. Chem.* **1998**, *37*, 4953.

(29) Frisch, M. J.; Trucks, G. W.; Schlegel, H. B.; Scuseria, G. E.; Robb, M. A.; Cheeseman, J. R.; Montgomery, Jr., J. A.; Vreven, T.; Kudin, K. N.; Burant, J. C.; Millam, J. M.; Iyengar, S. S.; Tomasi, J.; Barone, V.; Mennucci, B.; Cossi, M.; Scalmani, G.; Rega, N.; Petersson, G. A.; Nakatsuji, H.; Hada, M.; Ehara, M.; Toyota, K.; Fukuda, R.; Hasegawa, J.; Ishida, M.; Nakajima, T.; Honda, Y.; Kitao, O.; Nakai, H.; Klene, M.; Li, X.; Knox, J. E.; Hratchian, H. P.; Cross, J. B.; Bakken, V.; Adamo, C.; Jaramillo, J.; Gomperts, R.; Stratmann, R. E.; Yazyev, O.; Austin, A. J.; Cammi, R.; Pomelli, C.; Ochterski, J. W.; Ayala, P. Y.; Morokuma, K.; Voth, G. A.; Salvador, P.; Dannenberg, J. J.,; Zakrzewski, V. G.; Dapprich, S.; Daniels, A. D.; Strain, M. C.; Farkas, O.; Malick, D. K.; Rabuck, A. D.; Raghavachari, K.; Foresman, J. B.; Ortiz, J. V.; Cui, Q.; Baboul, A. G.; Clifford, S.; Cioslowski, J.; Stefanov, B. B.; Liu, G.; Liashenko, A.; Piskorz, P.; Komaromi, I.; Martin, R. L.; Fox, D. J.; Keith, T.; Al-Laham, M. A.; Peng, C. Y.; Nanayakkara, A.; Challacombe, M.; Gill, P. M. W.; Johnson, B.; Chen, W.; Wong, M. W.; Gonzalez, C.; Pople, J. A., *Gaussian09***;** Gaussian Inc.: Pittsburgh, PA, **2009**.

(30) Curtiss, L. A.; Redfern, P. C.; Raghavachari, K. *J. Chem. Phys.* **2007,** *126,* 084108.

(31) Fukui, K. *Acc. Chem. Res.* **1981,** *14,* 363.

(32) Truhlar, D. G.; Isaacson, A. D.; Garrett, B. C. In *Theory of Chemical Reaction Dynamics*; Baer, M., Ed.; CRC Press: Boca Raton, FL, 1985; p 65.

(33) Truhlar, D. G.; Garrett, B. C. *Acc. Chem. Res.* **1980,** *13,* 440.

(34) Chuang, Y.-Y.; Corchado, J. C.; Truhlar, D. G. *J. Phys. Chem. A.* **1999,** *103,* 1140.